Original Article

Microvascular morphology alteration using relaxation rate change with gadolinium-based magnetic resonance imaging contrast agent in patients with Alzheimer's disease

Xiao-Yi Guo[1]^, Hyeok Jung Kwon[2], Hak Young Rhee[3], Soonchan Park[4], Ah Rang Cho[5], Chang-Woo Ryu[4], Geon-Ho Jahng[4]^

[1]Department of Medicine, Graduate School, Kyung Hee University, Seoul, Republic of Korea; [2]Department of Medicine, College of Medicine, Kyung Hee University, Seoul, Republic of Korea; [3]Department of Neurology, Kyung Hee University Hospital at Gangdong, College of Medicine, Kyung Hee University, Seoul, Republic of Korea; [4]Department of Radiology, Kyung Hee University Hospital at Gangdong, College of Medicine, Kyung Hee University, Seoul, Republic of Korea; [5]Department of Psychiatry, Kyung Hee University Hospital at Gangdong, College of Medicine, Kyung Hee University, Seoul, Republic of Korea

Contributions: (I) Conception and design: GH Jahng; (II) Administrative support: XY Guo, HJ Kwon; (III) Provision of study materials or patients: HY Rhee, S Park, AR Cho, CW Ryu; (IV) Collection and assembly of data: HJ Kwon, HY Rhee, S Park, AR Cho, CW Ryu; (V) Data analysis and interpretation: XY Guo, HY Rhee, S Park, AR Cho, CW Ryu, GH Jahng; (VI) Manuscript writing: All authors; (VII) Final approval of manuscript: All authors.

Correspondence to: Geon-Ho Jahng, PhD. Department of Radiology, Kyung Hee University Hospital at Gangdong, College of Medicine, Kyung Hee University, 892 Dongnam-ro, Gangdong-Gu, Seoul 05278, Republic of Korea. Email: ghjahng@gmail.com.

Background: Conventional magnetic resonance imaging (MRI) techniques cannot demonstrate microvascular alterations in mild Alzheimer's disease (AD). Thus, the diagnosis of microvascular pathology commonly relies on postmortem. The purpose of this study was to evaluate alterations of microvascular structures in patients with AD using a 3T clinical MRI system with a commercially available contrast agent.

Methods: Eleven patients with AD and 11 cognitively normal (CN) controls were included in this cross-sectional prospective study. R2 and R2* relaxation rate changes (ΔR2 and ΔR2*) before and after a Gadolinium (Gd)-based contrast agent injection were calculated from images obtained with a multi-echo turbo spin-echo sequence and multi-echo gradient-echo sequence to obtain microvascular index maps of blood volume fraction (BVf), mean vessel diameter (mVD), vessel size index (VSI), mean vessel density (Q), and microvessel-weighted imaging (MvWI). Two-sample *t*-test was used to compare those values between the two groups. Correlation analysis was performed to evaluate the relationship between those values and age.

Results: BVfs at the corpus callosum and at the thalamus were significantly increased in the AD group (P=0.024 and P=0.005, respectively). BVf at the gray matter (P=0.020) and white matter area (P=0.012) were also significantly increased in the AD group compared with the CN group. MvWIs at the hippocampus and parahippocampal gyrus were significantly increased in the AD group compared with the CN group (P=0.020 and P=0.006, respectively). Voxel-based analysis showed both mVD and VSI were significantly decreased at the prefrontal lobe in the AD group. Q were not significant difference between CN and AD groups. MvWI were significantly positively correlated with age.

Conclusions: Microvascular index was a useful non-invasive method to evaluate microvascular morphology alteration. The microvascular morphology of AD was manifested as increasing BVf and microvessel-weighted.

^ ORCID: Xiao-Yi Guo, 0000-0003-4413-8362; Geon-Ho Jahng, 0000-0001-8881-1884.

Keywords: Microvascular index; Alzheimer's disease (AD); 3T magnetic resonance imaging (3T MRI); Gd-based contrast agent

Submitted May 25, 2022. Accepted for publication Sep 29, 2022. Published online Nov 01, 2022.
doi: 10.21037/qims-22-524
View this article at: https://dx.doi.org/10.21037/qims-22-524

Introduction

Alzheimer's disease (AD) is the most common progressive and complex age-related neurodegenerative disorder that can lead to cognitive decline (1) and memory loss (2). Concurrent cerebrovascular disease is common in patients with AD (3). This microvascular pathology is an important factor contributing to the worsening of AD through deteriorating microvascular hemodynamics leading to hypoxia, which in turn precipitates amyloid retention (4). Magnetic resonance imaging (MRI) is an important method if it can non-invasively map microvascular pathology in the AD brain.

The microvasculature consists of three types of small vessels: arterioles, capillaries, and venues. It maintains the blood-brain barrier (BBB). Information of microvessel densities and sizes are mostly provided by pathology after biopsy or samples extracted from clinics. Quantitative analysis of microvessel structures is an important method to demonstrate characteristics of brain diseases related to cerebrovascular disorders (5). MRI has been used to obtain information of microvessel structures. For example, previous studies have measured cerebral blood flow and blood volume to evaluate microvascular changes in AD (6,7). However, those values could not directly map microvascular changes, although those are valuable to evaluate alterations of blood flow and volume in AD brains. A more directly method based on measurement of relaxation rates has been introduced to map microvessel structures. Measuring transverse relaxation rate differences between before and after injection of a contrast agent, $\Delta R2$ and $\Delta R2^*$, has been applied to map microvessel structures of those with brain tumors (8), brain ischemic stroke (9), AD (10,11), and vascular dementia (12). In addition, researchers have further developed microvascular indices based on $\Delta R2$ and $\Delta R2^*$, including vessel size index (VSI) (13), mean vessel diameter (mVD) (14), microvascular density (Q) (15), blood volume fraction (BVf) (16), and microvessel-weighted imaging (MvWI) (17). Previous AD-model animal studies have shown that the microvascular indices of mVD, VSI, and Q have the characteristics of dynamically changes with age and disease progression (18). The other animal studies showed mVD and VSI increased in AD mice and Q has no changes (11).

Except our recent published paper which used gadolinium (Gd)-based contrast agent (12), most of previous studies were performed with using intravascular super-paramagnetic (SPION) and Manganese (Mn) contrast agents. These contrast agents are not immediately removed from the circulation by the reticuloendothelial system and have a longer plasma half-life (T1/2>2.5 h) (19), thus provide higher signal-to-noise (SNR) ratio, but have not recommended for human, yet. The characteristic of Gd-based contrast agent is double excretion of biliary system and renal system, excreting the contrast medium out of the body as soon as possible (20). It reduces the side effects caused by contrast medium residue in the body and is more suitable for clinical research. Relaxation rate differences as well as microvascular indices can provide useful quantitative metrics of *in vivo* vascular morphology (14), using a clinically approved contrast agent should be beneficial to directly apply it in clinics. To date, there are few studies on the use of Gd-based contrast agent in 3T MRI to research microvascular injuries of AD. Therefore, it is necessary to evaluate the value of microvascular mapping in clinical practice.

Despite its potential in the assessment of microvascular pathology, microvascular imaging has not been addressed in the diagnosis of AD in humanity to the best of our knowledge. Therefore, the objective of this study was to assess cerebral microvascular alterations in patients with AD relative to a cognitively normal (CN) population using *in vivo* microvascular index maps with Gd-based contrast agent in a 3T MRI system. We present the following article in accordance with the STROBE reporting checklist (available at https://qims.amegroups.com/article/view/10.21037/qims-22-524/rc).

Methods

Patient population

The study was conducted in accordance with the Declaration

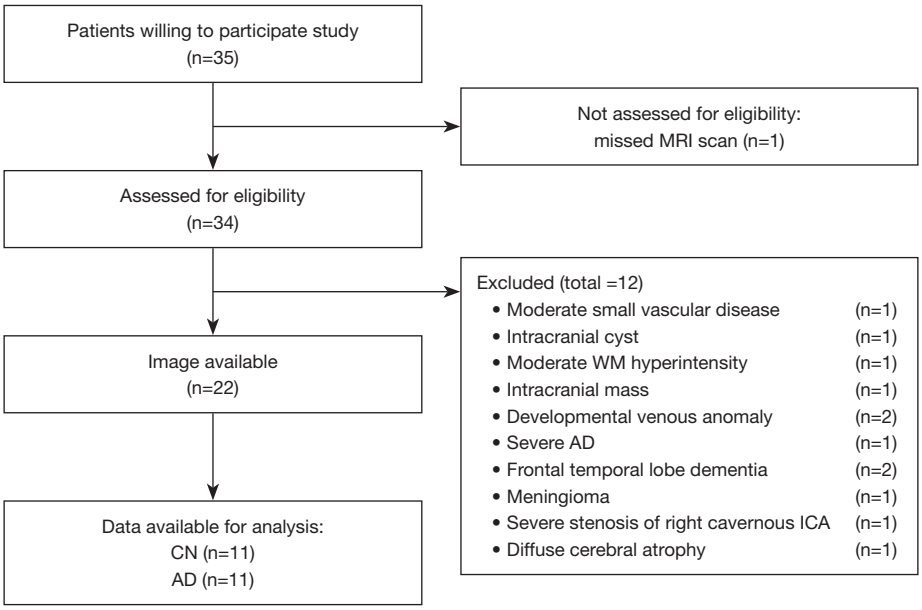

Figure 1 Participant recruitment and image screening flow diagram. MRI, magnetic resonance imaging; WM, white matter; AD, Alzheimer's disease; ICA, intracranial carotid artery; CN, cognitively normal elderly.

of Helsinki (as revised in 2013). Institutional review board of Kyung Hee University Hospital at Gangdong (2018-01-22–2020-01-21; No. KHNMC 2017-11-028) approved this cross-sectional prospective study. Informed consent was obtained from participants. Participants provided a detailed medical history. They underwent a neurologic examination, standard neuropsychological testing, and MRI scan. Cognitive function was assessed using the Seoul Neuropsychological Screening Battery (SNSB) (21) that covers five cognitive subsets: attention, memory, language, visuospatial function, and frontal/executive function as well as which was included in the Korean version of the Mini-Mental State Examination (MMSE) for global cognitive ability. Based on results of the SNSB examination and MRI findings, patients with probable AD were included in this study for the AD patient group. They had Clinical Dementia Rating (CDR) score of 0.5, 1, or 2 according to the criteria of the National Institute of Neurological and Communicative Disorders and the Stroke-Alzheimer Disease and Related Disorders Association (NINCDS–ADRDA) (21,22). Patients were excluded if they had evidence of intracranial diseases or if they had any other medical disorders severe enough to account for memory and related symptoms according to NINCDS–ADRDA criteria (22). *Figure 1* shows the screening process of participants: 35 participants were willing to participate in our study; 34 participants were enrolled in the study and completed the neurologic examination, standard neuropsychological testing, and MRI scan. Finally, we included 22 participants according to results of standard neuropsychological testing and MRI scan. We excluded 12 participants who had any other neurodegenerative disorders or intracranial diseases. A total of 22 participants, including 11 CN (CDR 0–0.5) and 11 AD (CDR 0.5–1) subjects recruited in the neurological center of our institution of Kyung Hee University Hospital at Gangdong were included in this study. There is no missing data in this study. A neurologist with 12 years of experience (HYR) and a psychiatrist with 16 years of experience (ARC) evaluated the SNSB examination. Two neuroradiologists with 10 and 16 years of experience (SP and CWR, respectively) evaluated brain MRI of each participant to detect any evidence of prior cortical infarctions or other space-occupying lesions. *Table 1* summarizes demographic characteristics and results of their neuropsychological tests.

MRI acquisition

Figure 2A shows the MRI scan protocol. MRI data were acquired using a 3T scanner (Ingenia, Philips Healthcare, The Netherlands) for all participants. First, to register microvascular index maps to a standard brain template,

Table 1 Statistical results of the demographic data and neuropsychological tests between the participant groups

Items	CN	AD	Statistics
Participants	11	11	22
Age (years)	70.0 (65.5 to 75.4)	80.0 (72.6 to 85.0)	P=0.013*, z=2.495
Sex (M/F)	11 (3/8)	11 (5/6)	P=0.637, χ^2=0.222
MMSE	28.0 (24.5 to 29.0)	21.0 (18.6 to 24.2)	P=0.002*, z=3.088
CDR	0 (0–0.5); CDR 0=9, CDR 0.5=2	1 (0.5–1); CDR 0.5=3, CDR 1=8	N/A

Age and MMSE: P value by Mann-Whitney test. Sex: P value by Chi-squared test. Age and MMSE scores are listed as median (95% CI for the median). CDR scores are presented as the median (range) value. *, P<0.05. CN, cognitively normal; AD, Alzheimer's disease; MMSE, Mini-Mental State Examination Score; CI, confidence interval; CDR, Clinical Demented Rating.

sagittal structural 3D T1-weighted (3DT1W) images were acquired before and after contrast injection with a turbo fast field echo sequence, similar to the magnetization-prepared rapid acquisition of the gradient echo (MPRAGE) sequence with the following parameters: repetition time (TR) =8.1 ms, echo time (TE) =3.7 ms, flip angle (FA) =8°, field-of-view (FOV) =236×236 mm^2, and voxel size =1×1×1 mm^3. This scan was repeated after admitting a contrast agent to examine any abnormality of the brain. Second, fluid-attenuated inversion recovery (FLAIR) image was acquired to calculate lesion probability map and examine any abnormality of the brain before admitting a contrast agent. Third, 3D time-of-flight (TOF) image was obtained to allow visual assessment of large vessel integrity before admitting a contrast agent. Fourth, a diffusion-weighted imaging (DWI) sequence based on spin-echo echo-planar imaging (EPI) was acquired with b=0 and 1,000 s/mm^2 to calculate the apparent diffusion coefficient (ADC) before admitting a contrast agent. ADC value was used to calculate VSI map. Finally, to map microvascular indices, a multi-echo (ME) turbo-spin-echo (TSE) sequence was scanned to calculate R2 relaxation rates before and after contrast injection. Imaging parameters for TSE imaging were as follows: TR =11,072 ms, TEs =16 ms +32 ms*n where n is the number of echoes, number of echoes =7, FOV =210×210 mm^2, acquisition voxel size =1.1×1.1×3 mm^3, reconstruction voxel size =0.4×0.4×3 mm^3, reconstruction matrix size =512×512, number of slices =45, TSE factor =14, and scan time =7 min 45 s. Furthermore, a multi-echo gradient-echo (GRE) sequence was also run to calculate R2* relaxation rates before and after contrast injection. Imaging parameters for GRE imaging were the same as those for TSE imaging except the following: TR =2,882 ms, TEs =2 ms +10 ms*n, n=7, FOV =210×210 mm^2, acquisition voxel size =1.1×1.1×3 mm^3, reconstruction voxel size =0.4×0.4×3 mm^3, reconstruction matrix size =512×512, number of slices =45, FA =60°, and scan time =4 min 43 s. A dose of 0.13 mL Gadobutrol (Gadovist, Bayer Schering Pharma AG, Berlin, Germany) per kg body weight was injected at a speed of 5 mL/s with a time delay of 18 s.

Mapping for microvascular imaging indices

Multi-echo TSE and GRE images before and after contrast injection were co-registered and resliced using the Statistical Parametric Mapping Version 12 (SPM12) software (http://www.fil.ion.ucl.ac.uk/spm/software/spm12/) to minimize motion during scans. The voxel-based R2* relaxation rates before (preR2*) and after (postR2*) contrast agent were calculated by fitting exponential decay curves from multi-echo GRE images. Then ΔR2* (i.e., postR2*- preR2*) was calculated by the difference in the relaxation rate between before and after contrast injection. We did not use the subtraction method of R2 relaxation rate to calculate ΔR2 because this method provided a poor resulting map. ΔR2 was calculated by using the signal ratio before and after contrast injection obtained from multi-echo TSE images proposed by Tropres *et al.* (23):

$$\Delta R2 = 1/TE \cdot \ln\left(S_{post}/S_{pre}\right) \quad [1]$$

Where S_{pre} and S_{post} were signal intensities obtained with TE =80 ms before and after injection of the contrast agent, respectively.

The following five microvascular indices were calculated based on ΔR2, ΔR2*, and ADC maps. First, the total blood volume fraction (BVf, %) in a voxel was calculated as follows, assuming that a voxel had thousands of microvessels and that it occupied a small blood fraction of the voxel volume (16):

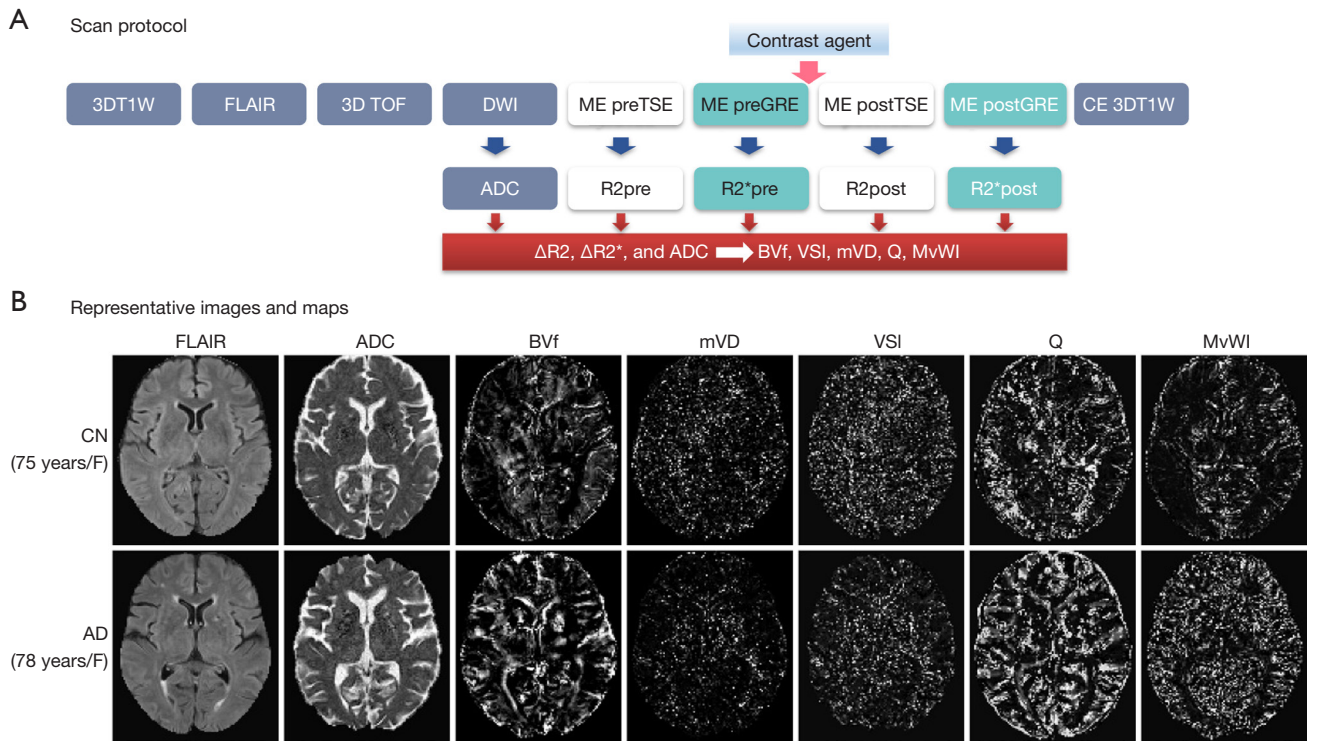

Figure 2 Scan protocol and representative images and maps. (A) Scan protocol with imaging acquisition sequences. R2 and R2* and ADC maps were calculated to map BVf, VSI, mVD, mean vessel density (Q), and MvWI. 3DT1W, 3D T1-weighted imaging; FLAIR, fluid attenuation inversion recovery to obtain white matter legion volume; 3D TOF, 3D Time-of-flight MR angiography to evaluate any large vessel integrity; DWI, DWI to calculate ADC; ME preSE, ME SE imaging before injection of contrast agent to map preR2 (relaxation rate); ME preGE, multi-echo GE imaging before injection of contrast agent to map preR2*; pre, imaging before injection of contrast agent; post, imaging after injection of contrast agent; CE using Gd-based contrast agent (Gadovist, Bayer Schering Pharma AG, Berlin, Germany). (B) Representative images and maps of the microvascular indices obtained from one CN participant (75-year-old female) and one AD patient (78-year-old female). The window level for each representative map was the same for both the CN and AD participant. ADC, apparent diffusion coefficient; BVf, blood volume fraction; VSI, vessel size index; mVD, mean vessel diameter; MvWI, microvessel-weighted imaging; DWI, diffusion-weighted imaging; ME, multi-echo; SE, spin-echo; GE, gradient-echo; CE, contrast enhancement; Gd, Gadolinium; CN, cognitively normal; AD, Alzheimer's disease.

$$BVf = 3/\left(4\pi\cdot\gamma\cdot\Delta\chi\cdot B_0\right)\cdot\Delta R2^*\cdot 100(\%) \quad [2]$$

where γ was the gyromagnetic ratio of hydrogen proton (Hz/T), B_0 was the strength of the main magnetic field (i.e., 3T), and Δχ (in cgs units) was the change in intravascular magnetic susceptibility due to the administration of the paramagnetic contrast agent. BVf was proportional to changes of ΔR2*. Note that Δχ depends on the type and concentration of the contrast agent. We used 0.2 ppm as the Δχ value. Second, the mVD (no unit) value in a voxel was calculated as follows (14):

$$mVD = \frac{\Delta R2^*}{\Delta R2} \quad [3]$$

mVD provides an estimate of microvascular changes. It is sensitive to the average vessel size in the voxel. It is valid for small coefficients of variation in vessel size distribution. Third, the VSI (expressed in μm) in a voxel was obtained from the following equation with the assumption that the microvasculature had a uniform distribution of randomly oriented straight cylinders as well as a small BVf (<<1) and a large echo time ($TE>>1/\left(2\pi\cdot\gamma\cdot\Delta\chi\cdot B_0\right)$) (13):

$$VSI = 0.424\cdot\left(\frac{ADC}{\gamma\cdot\Delta\chi\cdot B_0}\right)^{\frac{1}{2}}\cdot\left(\frac{\Delta R2^*}{\Delta R2}\right)^{\frac{3}{2}} \quad [4]$$

VSI is a characteristic of the distribution of the vessel

radii. It considers water diffusion rate (ADC: $\mu m^2/s$) and contrast agent concentration. Fourth, the mean vessel density (Q, expressed in $s^{-1/3}$) in a voxel was calculated as follows (15):

$$Q = \frac{\Delta R2}{(\Delta R2^*)^{\frac{2}{3}}} \quad [5]$$

Q was introduced to minimize the dependence of the contrast agent concentration. It is sensitive to intrinsic tissue properties. Therefore, Q is dependent on intrinsic tissue properties only. Finally, a MvWI (expressed in s^{-2}) in a voxel was calculated by using the following equation (17):

$$MvWI = \Delta R2 \times \Delta R2^* \quad [6]$$

MvWI was proposed to sensitively map small blood vessels.

Post-processing of microvascular index maps

We performed the following processing steps using SPM12 software. First, the 3DT1W image was segmented into different brain tissues using a Computational Anatomy Toolbox (CAT12) (http://www.neuro.uni-jena.de/cat/). It was spatially normalized to the dementia template generated by our lab (24). Second, co-registration was performed between 3DT1W image and the first-echo image of multi-echo GRE, all microvascular index maps, and FLAIR image. Third, all microvascular index maps and FLAIR image were spatially normalized into the dementia standard template using deformation field information of the 3DT1W image. Fourth, Gaussian smoothing was performed using the full-width at half maximum (FWHM) of $10\times10\times10$ mm^3 for voxel-based statistical analyses of all microvascular index maps.

Statistical analyses

Demographic data and descriptive clinical scores

Demographic data and descriptive clinical scores of all continuous variables such as age and MMSE scores were compared between the CN and AD groups using Mann-Whitney U-test. Sex was tested by the chi-squared test.

Voxel-based analyses

First, a voxel-based two-sample *t*-test was used to evaluate the difference of each microvascular index map between the two participant groups with age as a covariate. Second, voxel-based regression analysis was performed to evaluate the relationship between each microvascular index map and age without separating the two participant groups. Furthermore, voxel-based regression analysis was performed to evaluate the relationship between each microvascular index map and MMSE without separating the two participant groups with age as a covariate. Both analyses were performed to define atlas-based region-of-interests (ROIs). For both analyses, a significance level of α=0.001 was applied for clusters with at least 50 contiguous voxels without correction for multiple comparisons.

ROI-based analyses

ROI areas were defined based on both results of the voxel-based analysis and AD signature areas from previous reports as the hippocampus, parahippocampal gyrus, precuneus, caudate, corpus callosum, globus pallidus, lateral ventricle, putamen, and thalamus using wfu_pickAtlas software (https://www.nitrc.org/projects/wfu_pickatlas/). ROI values for each microvascular index map were extracted with a Marsbar toolbox (http://marsbar.sourceforge.net/). In addition, threshold-based ROIs were generated as more than 70% probability that a voxel is gray matter (GMV70) and more than 70% probability that a voxel is white matter (WMV70) to represent the dominant gray matter volume and the dominant white matter volume based on the brain tissue volume of 3DT1W image for each participant, respectively. In addition, areas at the white matter hyperintensity (WMHI) on FLAIR image were defined as ROIs by automatic segmentation with the lesion growth algorithm (25) as implemented in the LST toolbox version 3.0.0 (www.statisticalmodelling.de/lst.html) for SPM. ROI values for each microvascular index map were extracted from each ROI.

For ROI values, we performed the following analyses. First, Mann-Whitney U-test was used to explore differences of each microvascular index in each ROI between the two participant groups. Furthermore, to evaluate the influence in each microvascular index by the disease group and age, we performed the multiple regression analysis with each microvascular index as dependent variable and both the participant group and age as independent variables: each microvascular index = group + age. Second, rank correlation analysis was performed to evaluate the relationship between each microvascular index and subjects' age. Furthermore, partial correlation analysis was performed to evaluate the degree of relationship between each microvascular index and subjects' MMSE scores after adjusting for age in each ROI. Finally, Wilcoxon signed-rank test was used to compare

ROI values obtained from the three threshold-based ROIs of GMV70, WMV70, and WMHI in each participant group separately. For ROI analyses, the significant level was defined as α=0.05. All statistical analyses were performed using the Medcalc statistical program (MedCalc Software, Acacialaan, Ostend, Belgium).

Results

Figure 2B shows representative images and corresponding maps of FLAIR, ADC, and microvascular index maps of BVf, mVD, VSI, Q, and MvWI obtained from one CN participant (75-year-old female, CDR =0) and one AD patient (78-year-old female, CDR =1). We did not see any signals of microvascular indices at the CSF areas. By visual inspection, signals from BVf, Q and MvWI looked higher in AD than in CN. However, mVD and VSI signals looked lower in the AD than in the CN.

Demographic data and results of neuropsychological tests

Table 1 lists statistical analysis results of demographic data and results of neuropsychological tests for CN and AD groups. Age (P=0.013, z=2.495) was significantly different between the two groups. Sex (P=0.637, χ^2=0.222) was not significantly different between the two groups. MMSE was significantly different between the two groups (P=0.002, z=3.088), which was expected.

Voxel-based analysis of microvascular indices

Group difference

Figure 3A shows results of voxel-based two-sample t-test of microvascular index maps for between CN and AD groups. In summary, BVf and MvWI were higher while mVD and VSI were lower in the AD group than in the CN group. Q was not significant difference between two groups. Table S1 lists locations of significantly different results of the voxel-based group comparisons for each map. Results of comparisons of GMV and WMV are also listed in Table S1.

Multiple regression

Figure 3B shows results of voxel-based multiple regression analysis for microvascular index maps and age. In summary, microvascular indices of BVf, Q, and MvWI were significantly positively associated with age, but mVD was significantly negatively associated with age. VSI did not show any association with age. Table S2 lists locations of the significant relationship with age. All microvascular indices failed to show significant associations with MMSE scores.

ROI-based analysis of microvascular indices

Group comparison

Table 2 lists Mann-Whitney U-test results for each microvascular index between CN and AD groups. Compared with the CN group, BVf was significantly increased at the corpus callosum (P=0.024), thalamus (P=0.005), GMV70 (P=0.020), and WMV70 (P=0.012) in the AD group. MvWI was significantly increased at the hippocampus (P=0.020), parahippocampal gyrus (P=0.006), precuneus (P=0.008), globus pallidus (P=0.001), putamen (P=0.002), thalamus (P=0.020), GMV70 (P=0.003), WMV70 (P=0.005), and WMHI (P=0.017) in the AD group. *Table 2* lists results of comparisons of each microvascular index between CN and AD groups. Table S3 lists results of comparisons of ADC, ΔR2, ΔR2*, GMV, and WMV between CN and AD groups. GMV was significantly decreased in the AD group in the hippocampus and parahippocampal gyrus.

Multiple regression analysis

Results of the multiple regression are listed in *Table 2*. BVf significantly associated with the participant group in thalamus (F=4.860, P=0.029). MvWI significantly associated with the participant group in precuneus (F=4.289, P=0.029), globus pallidus (F=8.316, P=0.003), and WMV70 (F=10.529, P=0.001). Age was not associated with BVf value in any ROIs, but associated with MvWI values in hippocampus (F=9.297, P=0.002), putamen (F=19.964, P<0.0001), thalamus (F=6.460, P=0.007), and WMV70 (F=10.529, P=0.001). Results of the multiple regression analyses of ADC, ΔR2, and ΔR2* are listed in Table S3.

Correlation analysis

Figure 4 illustrates correlation heat map of each microvascular index and age (a), MMSE (b) in each ROIs. BVf was positively correlated with age at GMV70 (r=0.443, P=0.039) and WMV70 (r=0.449, P=0.036). Q was positively correlated with age at lateral ventricle (r=0.452, P=0.035). mVD was negatively correlated with age at WMHI (r=–0.439, P=0.041). MvWI was positively correlated with

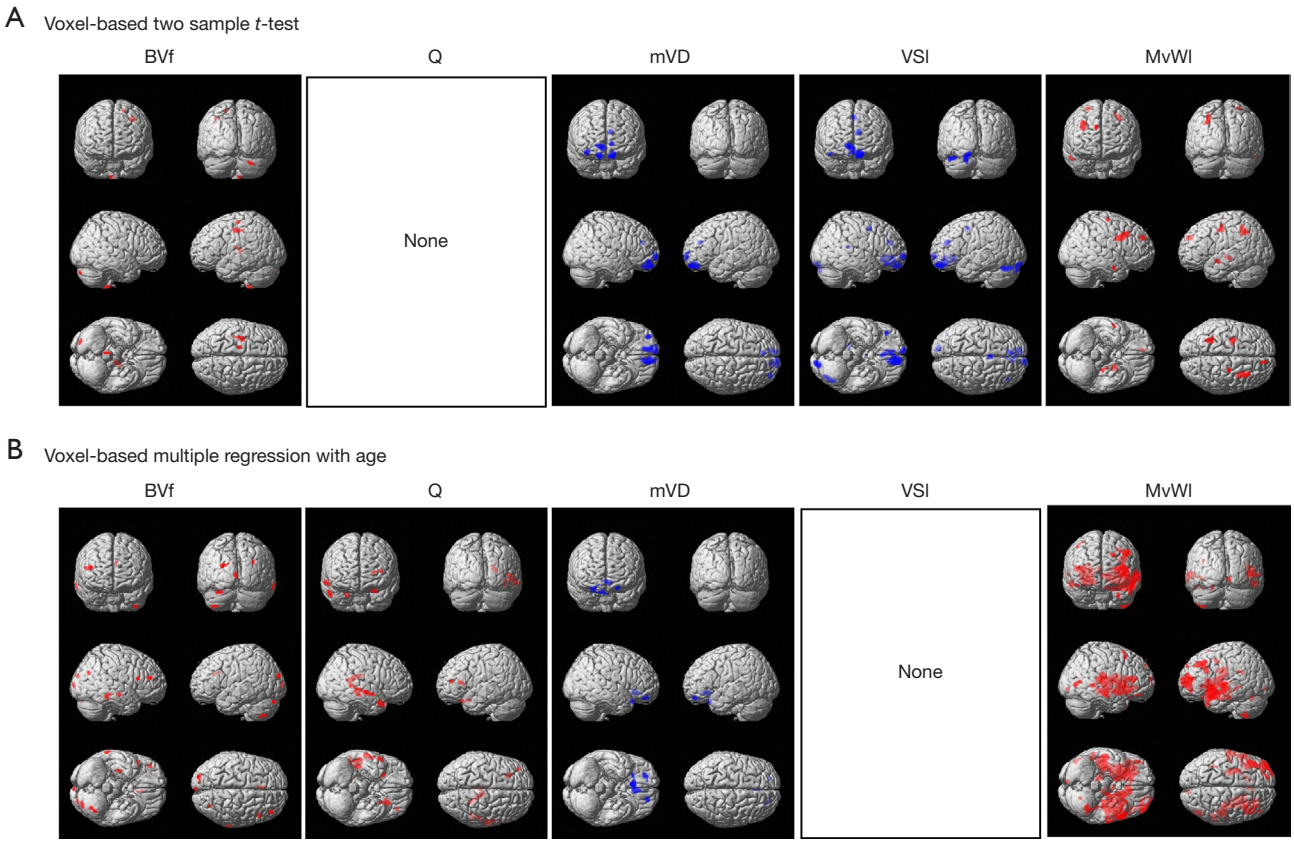

Figure 3 Result of voxel-based analyses of each microvascular index map. (A) Comparison between participant groups. The red color indicates greater microvascular index value in the AD than in CN group and the blue color indicates vice versa. (B) Multiple regression with age. The red color indicates the positive association with age, and the blue color indicates the negative association with age. None indicates no association between VSI and age. BVf, blood volume fraction; Q, mean vessel density; mVD, mean vessel diameter; VSI, vessel size index; MvWI, microvessel-weighted imaging; AD, Alzheimer's disease; CN, cognitive normal.

age at all ROIs (r>0.464, P<0.030), except precuneus. VSI were not significantly correlated with age. Only BVf was significant negatively correlated with MMSE at WMV70 (r=−0.445, P=0.043). Table S4 lists results of correlation analyses between ADC, ΔR2, ΔR2*, GMV, or WMV and age or MMSE score in each ROI.

Paired comparisons analysis

Figure 5 illustrates paired comparisons of microvascular indices among GMV70, WMV70, and WMHI ROIs in CN or AD participants. BVf was significantly higher in GMV70 than in WMV70 for both the CN (P=0.001) and AD (P=0.007) group. BVf also was significantly higher in WMV70 than in WMHI (P=0.001) for AD group. mVD was significantly higher in GMV70 than in WMV70 for CN (P=0.005) group, and higher in WMV70 than in WMHI for AD (P=0.042) group. VSI was significantly higher in WMHI than in WMV70 for only the CN group (P=0.010). Both Q and MvWI failed to show significant difference between GMV70 and WMV70 and between WMHI and WMV70 in both CN and AD groups. Table S5 lists results of paired comparisons of ADC, ΔR2, ΔR2* among GMV70, WMV70, and WMHI ROIs in CN or AD participants.

Discussion

Measurements of microvascular index changes were generally studied in tumor angiogenesis and microvascular remodeling of ischemic stroke. The morphological and structural changes of cerebral microvessels in patients with AD were rarely reported before. Cerebrovascular morphology and structure are crucial for the maintenance

Table 2 Results of comparisons of microvascular indices between the participant groups in specific brain areas and results of association between each microvascular index and the disease group and age

Microvascular index	ROI	CN	AD	*P value/ z-value	#F/P (group-p/age-p)
BVf (%)	Hippocampus	3.998 (3.046 to 5.345)	4.640 (3.827 to 4.928)	0.178/1.346	F=1.121/P=0.347 (0.376/0.632)
	Parahippocampal gyrus	3.545 (2.980 to 4.401)	4.289 (3.984 to 4.847)	0.061/1.871	F=2.485/P=0.110 (0.249/0.375)
	Precuneus	2.302 (1.824 to 2.905)	3.042 (2.144 to 3.504)	0.108/1.609	F=1.807/P=0.191 (0.315/0.459)
	Caudate	3.297 (2.490 to 4.694)	4.102 (2.814 to 5.226)	0.309/1.018	F=0.578/P=0.570 (0.231/0.749)
	Corpus callosum	2.780 (2.226 to 3.427)	3.747 (3.031 to 4.311)	0.024*/2.265	F=2.551/P=0.104 (0.071/0.955)
	Globus pallidus	3.901 (2.914 to 4.824)	5.376 (3.648 to 7.262)	0.082/1.740	F=2.463/P=0.112* (0.044*/0.448)
	Lateral ventricle	3.099 (2.580 to 3.856)	3.369 (2.991 to 4.552)	0.178/1.346	F=0.548/P=0.587 (0.369/0.366)
	Putamen	3.416 (2.892 to 4.768)	4.431 (3.722 to 5.414)	0.082/1.740	F=1.523/P=0.244 (0.266/0.652)
	Thalamus	2.893 (2.332 to 3.469)	3.801 (3.610 to 4.329)	0.005*/2.791	F=4.860/P=0.020* (0.014*/0.818)
	GMV70	3.270 (2.862 to 3.688)	3.843 (3.447 to 4.786)	0.020*/2.331	F=4.275/P=0.029* (0.116/0.286)
	WMV70	2.620 (2.223 to 3.201)	3.743 (3.042 to 4.055)	0.012*/2.528	F=4.211/P=0.031* (0.070/0.466)
	WMHI	2.201 (1.712 to 2.514)	2.669 (1.927 to 3.274)	0.108/1.609	F=0.731/P=0.494 (0.244/0.448)
Q ($s^{-1/3}$)	Hippocampus	2.705 (1.494 to 2.862)	2.263 (2.043 to 2.677)	0.870/0.164	F=2.558/P=0.104 (0.358/0.038*)
	Parahippocampal gyrus	2.701 (1.769 to 2.975)	2.417 (2.146 to 2.743)	0.818/0.230	F=0.2775/P=0.090 (0.217/0.030*)
	Precuneus	2.221 (1.800 to 2.813)	2.167 (1.990 to 3.007)	0.870/0.164	F=1.047/P=0.370 (0.687/0.183)
	Caudate	2.957 (1.585 to 3.420)	2.7858 (1.973 to 3.444)	0.922/0.099	F=1.854/P=0.184 (0.435/0.073)
	Corpus callosum	2.768 (1.851 to 3.162)	2.614 (1.924 to 2.962)	0.622/0.492	F=3.786/P=0.041* (0.141/0.013*)
	Globus pallidus	2.598 (1.698 to 3.002)	2.479 (2.055 to 3.004)	0.922/0.099	F=1.836/P=0.187 (0.281/0.071)
	Lateral ventricle	3.023 (1.745 to 3.606)	2.373 (2.172 to 3.531)	0.768/0.295	F=4.023/P=0.035* (0.268/0.012*)
	Putamen	2.514 (1.717 to 2.848)	2.474 (1.929 to 2.826)	0.974/0.033	F=1.608/P=0.226 (0.541/0.097)
	Thalamus	2.527 (1.861 to 3.357)	2.122 (1.899 to 2.946)	0.670/0.427	F=1.191/P=0.326 (0.250/0.155)
	GMV70	2.655 (1.792 to 2.739)	2.326 (2.124 to 2.522)	0.718/0.361	F=1.442/P=0.261 (0.465/0.109)
	WMV70	2.731 (1.961 to 3.225)	2.273 (1.974 to 2.804)	0.491/0.689	F=3.286/P=0.060 (0.104/0.020*)
	WMHI	2.630 (1.645 to 3.297)	2.519 (1.970 to 2.891)	0.718/0.361	F=1.257/P=0.307 (0.282/0.136)
mVD (a.u.)	Hippocampus	3.943 (2.307 to 4.016)	2.996 (2.190 to 3.878)	0.375/0.886	F=0.388/P=0.684 (0.552/0.846)
	Parahippocampal gyrus	3.468 (2.290 to 3.662)	3.033 (2.240 to 3.616)	0.622/0.492	F=0.179/P=0.837 (0.900/0.682)
	Precuneus	2.471 (2.010 to 2.584)	1.679 (1.451 to 2.614)	0.279/1.083	F=0.326/P=0.726 (0.661/0.759)
	Caudate	3.599 (2.317 to 4.393)	3.067 (2.532 to 3.281)	0.341/0.952	F=1.568/P=0.234 (0.945/0.168)
	Corpus callosum	2.838 (2.166 to 3.398)	2.644 (2.076 to 3.121)	0.375/0.886	F=0.701/P=0.508 (0.795/0.282)
	Globus pallidus	3.686 (3.039 to 3.846)	3.705 (2.557 to 4.220)	0.533/0.624	F=0.090/P=0.914 (0.713/0.971)
	Lateral ventricle	3.040 (2.141 to 3.783)	2.516 (2.1550 to 2.998)	0.491/0.689	F=1.648/P=0.219 (0.620/0.100)
	Putamen	3.863 (3.092 to 4.005)	3.631 (2.798 to 3.957)	0.768/0.295	F=0.021/P=0.980 (0.879/0.847)
	Thalamus	3.081 (2.470 to 3.723)	3.353 (2.216 to 3.864)	0.279/1.083	F=0.744/P=0.489 (0.273/0.325)
	GMV70	3.340 (2.297 to 3.706)	2.624 (2.097 to 3.325)	0.279/1.083	F=0.232/P=0.796 (0.809/0.700)
	WMV70	2.867 (2.279 to 3.115)	2.746 (2.118 to 3.265)	0.768/0.295	F=0.188/P=0.830 (0.682/0.552)
	WMHI	2.958 (2.238 to 3.161)	2.245 (1.893 to 2.966)	0.123/1.543	F=1.674/P=0.214 (0.910/0.130)

Table 2 (*continued*)

Table 2 (*continued*)

Microvascular index	ROI	CN	AD	*P value/ z-value	#F/P (group-p/age-p)
VSI (μm)	Hippocampus	7.720 (5.729 to 8.482)	6.665 (5.372 to 7.714)	0.224/1.215	F=0.549/P=0.587 (0.321/0.722)
	Parahippocampal Gyrus	7.024 (5.683 to 7.693)	6.613 (5.600 to 7.620)	0.718/0.361	F=0.042/P=0.959 (0.776/0.864)
	Precuneus	6.240 (5.301 to 6.424)	5.559 (3.939 to 6.547)	0.251/1.149	F=0.922/P=0.415 (0.202/0.638)
	Caudate	7.906 (6.349 to 8.576)	7.385 (5.747 to 8.212)	0.224/1.215	F=0.556/P=0.583 (0.435/0.898)
	Corpus callosum	7.516 (6.354 to 7.875)	6.857 (5.776 to 7.683)	0.375/0.886	F=0.453/P=0.642 (0.411/0.926)
	Globus pallidus	6.893 (6.118 to 7.165)	7.501 (5.586 to 7.864)	0.200/1.280	F=0.552/P=0.585 (0.374/0.945)
	Lateral ventricle	7.680 (6.463 to 8.710)	6.822 (5.905 to 7.440)	0.158/1.412	F=1.210/P=0.320 (0.341/0.647)
	Putamen	7.346 (6.736 to 7.659)	7.641 (5.821 to 8.329)	0.491/0.689	F=0.145/P=0.866 (0.862/0.749)
	Thalamus	7.265 (6.534 to 7.968)	7.385 (5.512 to 7.977)	0.768/0.295	F=0.007/P=0.993 (0.982/0.914)
	GMV70	6.805 (5.476 to 7.479)	6.126 (4.990 to 7.465)	0.341/0.952	F=1.096/P=0.354 (0.164/0.302)
	WMV70	6.745 (5.719 to 6.969)	6.237 (5.480 to 7.752)	0.974/0.033	F=0.021/P=0.979 (0.982/0.877)
	WMHI	7.071 (6.284 to 7.901)	6.083 (4.990 to 6.726)	0.071/1.806	F=1.486/P=0.251 (0.235/0.746)
MvWI (s^{-2})	Hippocampus	6.579 (5.298 to 6.958)	9.175 (5.948 to 11.249)	0.020*/2.331	F=9.297/P=0.002* (0.156/0.020*)
	Parahippocampal gyrus	6.506 (5.725 to 7.058)	9.074 (6.772 to 11.801)	0.006*/2.725	F=9.581/P=0.001* (0.055/0.051)
	Precuneus	4.555 (3.417 to 6.078)	8.495 (5.959 to 10.145)	0.008*/2.659	F=4.289/P=0.029* (0.041*/0.695)
	Caudate	5.890 (4.916 to 7.711)	7.901 (6.842 to 10.198)	0.053/1.937	F=4.337/P=0.028* (0.368/0.086)
	Corpus callosum	5.347 (4.518 to 7.396)	8.372 (5.136 to 9.923)	0.053/1.937	F=5.379/P=0.014* (0.279/0.066)
	Globus pallidus	6.856 (5.729 to 8.579)	10.290 (8.540 to 11.813)	0.001*/3.250	F=8.316/P=0.003* (0.016*/0.284)
	Lateral ventricle	5.917 (5.254 to 8.287)	7.605 (4.883 to 10.285)	0.279/1.083	F=2.219/P=0.136 (0.878/0.113)
	Putamen	6.304 (4.191 to 8.492)	10.020 (8.320 to 10.777)	0.002*/3.119	F=19.964/P<0.001* (0.061/0.001*)
	Thalamus	5.683 (4.513 to 6.493)	6.716 (6.088 to 8.628)	0.020*/2.331	F=6.460/P=0.007 (0.258/0.042*)
	GMV70	5.145 (4.850 to 6.825)	9.162 (7.200 to 9.653)	0.003*/2.988	F=8.786/P=0.002* (0.052/0.076)
	WMV70	5.047 (4.170 to 6.037)	7.536 (5.045 to 9.418)	0.005*/2.791	F=10.529/P=0.001* (0.049*/0.039*)
	WMHI	3.915 (3.020 to 5.711)	6.912 (4.419 to 8.720)	0.017*/2.397	F=3.786/P=0.041* (0.101/0.417)

*, P value by Mann-Whitney U-test and data are listed as median (95% CI for the median). #, F and P values by multiple regression analysis with modeling as each microvascular index = participant group + age. ROI, region of interest; CN, cognitively normal; AD, Alzheimer's disease; BVf, blood volume fraction; Q, mean vessel density; mVD, mean vessel diameter; VSI, vessel size index; MvWI, microvessel-weighted imaging; GMV70, more than 70% gray matter volume; WMV70, more than 70% white matter volume; WMHI, white matter hyperintensity.

of cognitive functions during aging and in AD, because cerebrovascular alterations may alter vascular integrity and blood supply. We investigated alterations of microvascular morphology and structure in AD and CN participants using relaxation rate difference obtained before and after injection of a clinically available Gd-based contrast agent with a clinical 3T MRI system. We found the following results. First, ROI-based comparison showed that BVf and MvWI were increased in AD patients compared with CN participants, but, Q, mVD, and VSI were not increased or decreased in AD patients depending on brain area. Second, voxel-based analysis showed mVD, and VSI were decreased in the prefrontal lobe. Finally, BVf and mVD in the WMHI area was significantly decreased compared to that in the WMV70 area in AD participants.

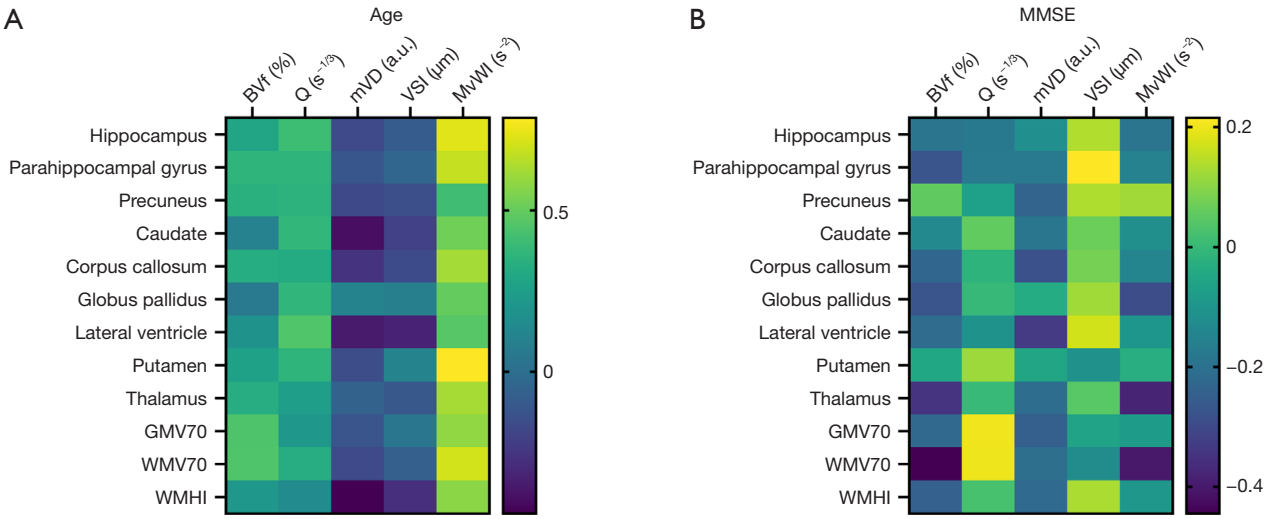

Figure 4 Correlation heat map in each brain area. (A) Between each microvascular index and age. (B) Between each microvascular index and MMSE. Color coding indicates the strength of correlation between microvascular index and age or MMSE. BVf, blood volume fraction; Q, mean vessel density; mVD, mean vessel diameter; VSI, vessel size index; MvWI, microvessel-weighted imaging, GMV70, more than 70% gray matter volume; WMV70, more than 70% white matter volume; WMHI, white matter hyperintensity; MMSE, mini-mental state examination.

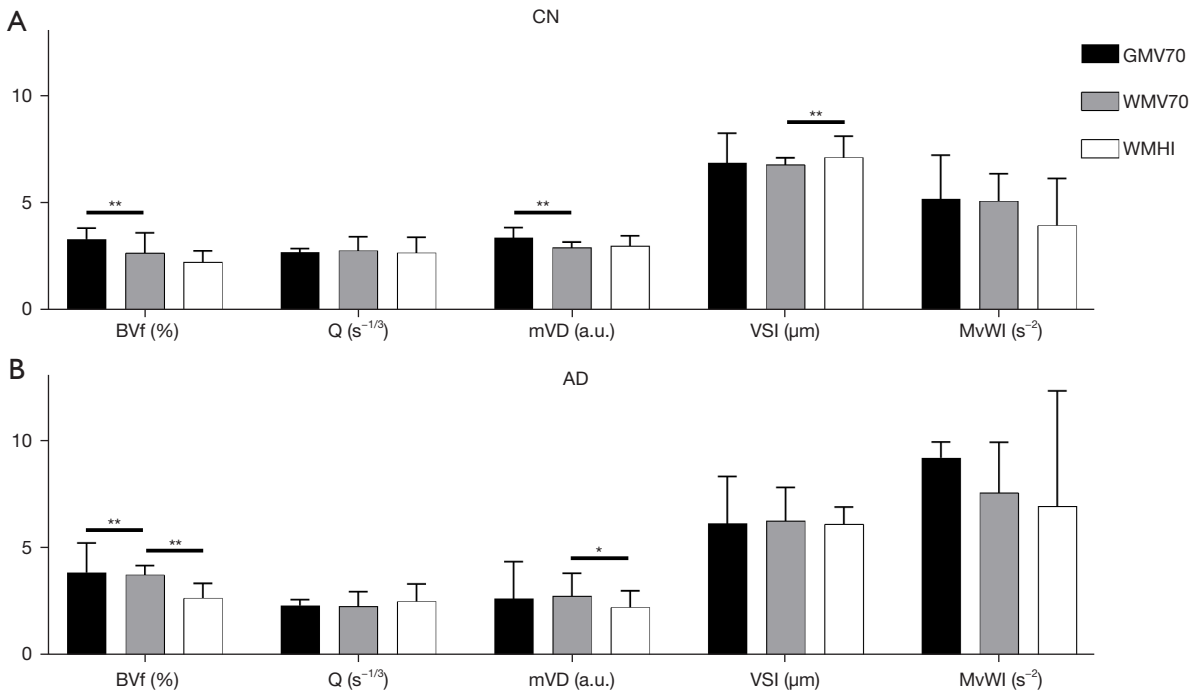

Figure 5 The paired comparisons of microvascular indices among GMV70, WMV70, and WMHI ROIs. (A) CN group. (B) AD group. The dark bar indicates the GMV70, the grey bar indicates the WMV70, and the white bar indicates the WMHI. The bar shows as median (95% CI for the median). *, P<0.05, **, P<0.01. CN, cognitively normal; AD, Alzheimer's disease; GMV70, brain area of more than 70% of gray matter volume; WMV70, brain area of more than 70% of white matter volume; WMHI, white matter hyperintensity on FLAIR; BVf, blood volume fraction; Q, mean vessel density; mVD, mean vessel diameter; VSI, vessel size index; MvWI, microvessel-weighted imaging; ROI, region of interest.

Microvessel quantity increased in AD patients

BVf is the portion of tissue occupied by blood, characterizing angiogenesis (26,27). BVf was commonly used to monitor angiogenesis in tumor or bone regeneration studies (28,29). In this study, BVf index was used to detect alteration of cerebral microvascular. Increased BVf may indicate more neovascularization in the AD condition. The proliferation of microvessels may be related to the deposition of amyloid protein in the patient's brain. Aβ is a modulator of vessel density and vascular remodeling through angiogenic mechanisms. Previous studies showed that microvessel amount in the Tg4510 (15-mo-old) was increased compared with that in normal mice using two-photon microscopy (30), and MRI reported a microvascular density increased in the APP23 (14-mo-old) (18). However, vascular density in AD patients was decreased compared with normal elderly based on postmortem analysis (31). Such discrepancies between the previous postmortem study and this study might be explained by variation in disease stage. Microvessel density could change depending on the disease stage. It could show a transient increase or a decrease depending on AD progression. Microvessel density values are generally significantly reduced in the late stage of Aβ pathology (32). Our study reported that the directly related index Q with density was no significant difference in the AD condition. However, the index BVf and MvWI, which can indirectly reflect the microvessel quantity was increased. It is unclear if the increased vessel density in human brain and animal will lead to abnormal or loss of physiologic function. Thus, further studies are required to assess which vascular index is more sensitive to density and the effect of AD progression on microvascular density.

This study showed that MvWI increased in AD patients, especially in the hippocampus, parahippocampal gyrus. MvWI was introduced to improve the sensitivity to map intercortical penetrating arterioles and deep venules within the brain while simultaneously reducing the vessel size overestimation by multiplication of ΔR2 and ΔR2*. It is unclear which one of ΔR2 and/or ΔR2* dominantly contributes to the increase of MvWI value in patients with AD. ΔR2 is widely used to detect cerebral arterioles and venules because it is less susceptible to air tissue interface artifacts (17). ΔR2* is sensitively mapped to relatively large vessels.

Microvessel diameter changes

mVD is a dimensionless parameter, qualitatively measures the mean vessel diameter, and represents the distribution of a vascular size. Unfortunately, this quantitative ROI-based analysis did not find a significantly increase or decrease in the mVD in Alzheimer's susceptible areas such as the parahippocampal gyrus and hippocampus. However, voxel-based analysis suggested that both mVD and VSI in the prefrontal regions decreased significantly. A review indicates that executive abilities depend on prefrontal areas (33). Therefore, the decrease of prefrontal vessel diameter may be the reason for the slow metabolism and implicated in executive dysfunction in AD. An animal micro-optical sectioning also concluded that the microvessel diameter of AD was decreased (34). In addition, tau overexpressing changes blood vessel morphology, including the abnormal structure and spiraling morphologies (30). Another previously animal study also showed that the vascular diameter of APP23 mice underwent a morphology variation from slight constriction in the early stage to obvious dilation in the late stage of AD (18). In the early phase of AD, the deposition of Aβ peptides can lead to hypoxia and hypoperfusion, resulting in the vasoconstriction by the regulation of vascular contractile endothelin-1 and angiotensin II (35,36). As the disease continues to advance, the serious Aβ pathological deposition contributes to the vascular elasticity loss and degeneration of the vascular smooth muscle cell. It enables the inner surface of the vascular lumen to be rugged, eventually enabling vascular to dilate (34,35). A significant dilation generally exists in the late stage of AD (18). VSI is also usually used to monitor the contraction and dilation of microvessels. It is more quantitative than mVD due to considering the contrast agent concentration water apparent diffusion rate and magnetic field intensity. The variation of VSI values was generally consistent with mVD.

Difference of microvascular index between GMV and WMV or between WMV and WMHI

BVf, and mVD value were higher in dominant gray matter areas than in dominant white matter areas of brains for CN participants, indicating that the blood supply or vascular distribution and vessel structure in the brain was

not uniform and the microvascular distribution within the white matter was relatively less. Thus, white matter is more vulnerable to chronic hypoperfusion and hypoxic-ischemic injury than gray matter (37). In the AD group, this difference still exists. The difference of BVf between GMV70 and WMV70 was 0.670 for the CN group and 0.100 for the AD group, indicating the microvascular structure in the white matter area was destructed in AD patients.

WMHI on FLAIR image reflects neuropathological substrates or tissue damage with varying severity. Compared to the normal white matter (WMV70) area, VSI was increased in the WMHI area of CN participants. However, BVf was not changed, indicating that the alteration of microvascular structure was a normal function in the WMHI area and a compensative vasodilation to maintain normal blood supply. However, in the AD group, BVf in the WMHI area was significantly decreased compared to that in the WMV70 area (P=0.001), and mVD also significantly decreased. Therefore, it can be considered that the pathological mechanism WMHI in the brain of patients with AD is completely different from that of normal population. WMHI area in the normal elderly is associated with damage caused by demyelinate, axonal loss, and enlarged perivascular spaces (38), while WMHI in AD is often associated with damage caused by neuronal loss and microvascular injury evolved by microglia activation (39). Therefore, when the BVf in the WMHI area decreased accompany with vasoconstriction, it might be considered that it is caused by AD pathology.

Limitation of this study

Our study has several limitations. First, microvascular alterations were not confirmed with autopsy or pathological diagnosis. Second, the sample size for each group was too small and age was younger in the CN group. During the voxel-based analysis, we always used age as a covariate. Results of the voxel-based two-sample *t*-test showed that both BVf and MvWI are still significantly different between the two groups, indicating that both indices are demonstrated the microstructure changes in AD patients. In a future study, it should be better to match ages for both groups. Third, in the AD group, we only included mild AD patients (CDR 0.5–1), no severe AD include, that might have further changes of microvascular morphology caused by plaque-related inflammation and anti-inflammatory cytokine interleukin expression (40). Fourth, since this was a cross-sectional study, values of microvascular indices for predicting progression from CN to AD were not assessed. Furthermore, this study performed by 3T clinical MRI, the SNR ratio was lower than the high magnetic field (7T, 9.3T) used in previous animal experiments. Finally, compared with contrast agents used in animal experiments Mn and USPIO, the half-life of contrast agent Gd-based is shorter and can be excreted from the body quickly.

Conclusions

This is the first study to evaluate cerebral microvascular alterations in patients with AD using microvascular indices obtained with the relaxation rate difference before and after injection of a Gd-based contrast agent in 3T clinical MRI. We found that BVf and MvWI were increased in AD patients, mVD and VSI were decreased in the prefrontal lobe in AD patients. In addition, the BVf and mVD in the WMHI area was significantly decreased in AD patients. We can conclude that some microvascular indices might be useful as imaging biomarkers to evaluate the alteration of brain microstructure in AD. However, additional studies with a relatively large sample size are needed to validate our findings.

Acknowledgments

The authors appreciate Miss Seon Hwa Lee (Clinical Research Institute, Kyung Hee University Hospital at Gangdong, Seoul, Korea) for providing advice on the statistical analyses.

Funding: This research was supported by Basic Science Research Program through the National Research Foundation of Korea (NRF) funded by the Ministry of Education (No. 2016R1D1A1B03930720 to GH Jahng) and by the National Research Foundation of Korea (NRF) grant funded by the Ministry of Science and ICT (No. 2020R1A2C100474912 to GH Jahng).

Footnote

Reporting Checklist: The authors have completed the STROBE reporting checklist. Available at https://qims.amegroups.com/article/view/10.21037/qims-22-524/rc

Conflicts of Interest: All authors have completed the ICMJE uniform disclosure form (available at https://qims.amegroups.com/article/view/10.21037/qims-22-524/coif).

The authors have no conflicts of interest to declare.

Ethical Statement: The authors are accountable for all aspects of the work in ensuring that questions related to the accuracy or integrity of any part of the work are appropriately investigated and resolved. The study was conducted in accordance with the Declaration of Helsinki (as revised in 2013) and approved by the Institutional Review Board of Kyung Hee University Hospital at Gangdong, Seoul, Republic of Korea (2018-01-22–2020-01-21; No. KHNMC 2017-11-028). Informed consent was obtained from participants.

References

1. Albertini V, Benussi L, Paterlini A, Glionna M, Prestia A, Bocchio-Chiavetto L, Amicucci G, Galluzzi S, Adorni A, Geroldi C, Binetti G, Frisoni GB, Ghidoni R. Distinct cerebrospinal fluid amyloid-beta peptide signatures in cognitive decline associated with Alzheimer's disease and schizophrenia. Electrophoresis 2012;33:3738-44.
2. Jahn H. Memory loss in Alzheimer's disease. Dialogues Clin Neurosci 2013;15:445-54.
3. Toledo JB, Arnold SE, Raible K, Brettschneider J, Xie SX, Grossman M, Monsell SE, Kukull WA, Trojanowski JQ. Contribution of cerebrovascular disease in autopsy confirmed neurodegenerative disease cases in the National Alzheimer's Coordinating Centre. Brain 2013;136:2697-706.
4. Ewers M, Mielke MM, Hampel H. Blood-based biomarkers of microvascular pathology in Alzheimer's disease. Exp Gerontol 2010;45:75-9.
5. Hunter JM, Kwan J, Malek-Ahmadi M, Maarouf CL, Kokjohn TA, Belden C, Sabbagh MN, Beach TG, Roher AE. Morphological and pathological evolution of the brain microcirculation in aging and Alzheimer's disease. PLoS One 2012;7:e36893.
6. Weidensteiner C, Metzger F, Bruns A, Bohrmann B, Kuennecke B, von Kienlin M. Cortical hypoperfusion in the B6.PS2APP mouse model for Alzheimer's disease: comprehensive phenotyping of vascular and tissular parameters by MRI. Magn Reson Med 2009;62:35-45.
7. Nielsen RB, Parbo P, Ismail R, Dalby R, Tietze A, Brændgaard H, Gottrup H, Brooks DJ, Østergaard L, Eskildsen SF. Impaired perfusion and capillary dysfunction in prodromal Alzheimer's disease. Alzheimers Dement (Amst) 2020;12:e12032.
8. Farrar CT, Kamoun WS, Ley CD, Kim YR, Kwon SJ, Dai G, Rosen BR, di Tomaso E, Jain RK, Sorensen AG. In vivo validation of MRI vessel caliber index measurement methods with intravital optical microscopy in a U87 mouse brain tumor model. Neuro Oncol 2010;12:341-50.
9. Kang M, Jin S, Lee D, Cho H. MRI Visualization of Whole Brain Macro- and Microvascular Remodeling in a Rat Model of Ischemic Stroke: A Pilot Study. Sci Rep 2020;10:4989.
10. Zerbi V, Jansen D, Dederen PJ, Veltien A, Hamans B, Liu Y, Heerschap A, Kiliaan AJ. Microvascular cerebral blood volume changes in aging APP(swe)/PS1(dE9) AD mouse model: a voxel-wise approach. Brain Struct Funct 2013;218:1085-98.
11. Chang SK, Kim J, Lee D, Yoo CH, Jin S, Rhee HY, Ryu CW, Lee JK, Cho H, Jahng GH. Mapping of microvascular architecture in the brain of an Alzheimer's disease mouse model using MRI. NMR Biomed 2021;34:e4481.
12. Choi HI, Ryu CW, Kim S, Rhee HY, Jahng GH. Changes in Microvascular Morphology in Subcortical Vascular Dementia: A Study of Vessel Size Magnetic Resonance Imaging. Front Neurol 2020;11:545450.
13. Troprès I, Grimault S, Vaeth A, Grillon E, Julien C, Payen JF, Lamalle L, Décorps M. Vessel size imaging. Magn Reson Med 2001;45:397-408.
14. Dennie J, Mandeville JB, Boxerman JL, Packard SD, Rosen BR, Weisskoff RM. NMR imaging of changes in vascular morphology due to tumor angiogenesis. Magn Reson Med 1998;40:793-9.
15. Jensen JH, Chandra R. Strong field behavior of the NMR signal from magnetically heterogeneous tissues. Magn Reson Med 2000;43:226-36.
16. Yablonskiy DA, Haacke EM. Theory of NMR signal behavior in magnetically inhomogeneous tissues: the static dephasing regime. Magn Reson Med 1994;32:749-63.
17. Jung HS, Jin SH, Cho JH, Han SH, Lee DK, Cho H. UTE-ΔR2 -ΔR2 * combined MR whole-brain angiogram

using dual-contrast superparamagnetic iron oxide nanoparticles. NMR Biomed 2016;29:690-701.
18. Xu X, Meng T, Wen Q, Tao M, Wang P, Zhong K, Shen Y. Dynamic changes in vascular size and density in transgenic mice with Alzheimer's disease. Aging (Albany NY) 2020. [Epub ahead of print]. doi: 10.18632/aging.103672.
19. Ullrich RT, Jikeli JF, Diedenhofen M, Böhm-Sturm P, Unruh M, Vollmar S, Hoehn M. In-vivo visualization of tumor microvessel density and response to anti-angiogenic treatment by high resolution MRI in mice. PLoS One 2011;6:e19592.
20. Do C, DeAguero J, Brearley A, Trejo X, Howard T, Escobar GP, Wagner B. Gadolinium-Based Contrast Agent Use, Their Safety, and Practice Evolution. Kidney360 2020;1:561-8.
21. Ahn HJ, Chin J, Park A, Lee BH, Suh MK, Seo SW, Na DL. Seoul Neuropsychological Screening Battery-dementia version (SNSB-D): a useful tool for assessing and monitoring cognitive impairments in dementia patients. J Korean Med Sci 2010;25:1071-6.
22. Dubois B, Feldman HH, Jacova C, Dekosky ST, Barberger-Gateau P, Cummings J, Delacourte A, Galasko D, Gauthier S, Jicha G, Meguro K, O'brien J, Pasquier F, Robert P, Rossor M, Salloway S, Stern Y, Visser PJ, Scheltens P. Research criteria for the diagnosis of Alzheimer's disease: revising the NINCDS-ADRDA criteria. Lancet Neurol 2007;6:734-46.
23. Troprès I, Pannetier N, Grand S, Lemasson B, Moisan A, Péoc'h M, Rémy C, Barbier EL. Imaging the microvessel caliber and density: Principles and applications of microvascular MRI. Magn Reson Med 2015;73:325-41.
24. Guo XY, Chang Y, Kim Y, Rhee HY, Cho AR, Park S, Ryu CW, San Lee J, Lee KM, Shin W, Park KC, Kim EJ, Jahng GH. Development and evaluation of a T1 standard brain template for Alzheimer disease. Quant Imaging Med Surg 2021;11:2224-44.
25. Schmidt P, Gaser C, Arsic M, Buck D, Förschler A, Berthele A, Hoshi M, Ilg R, Schmid VJ, Zimmer C, Hemmer B, Mühlau M. An automated tool for detection of FLAIR-hyperintense white-matter lesions in Multiple Sclerosis. Neuroimage 2012;59:3774-83.
26. Seevinck PR, Deddens LH, Dijkhuizen RM. Magnetic resonance imaging of brain angiogenesis after stroke. Angiogenesis 2010;13:101-11.
27. Ungersma SE, Pacheco G, Ho C, Yee SF, Ross J, van Bruggen N, Peale FV Jr, Ross S, Carano RA. Erratum to: Ungersma SE, Pacheco G, Ho C, Yee SF, Ross J, van Bruggen N, Peale FV Jr, Ross S, Carano RA. Vessel imaging with viable tumor analysis for quantification of tumor angiogenesis. Magn Reson Med 2010;63:1637–1647. Magn Reson Med 2011;65:889-99.
28. Righesso LAR, Terekhov M, Götz H, Ackermann M, Emrich T, Schreiber LM, Müller WEG, Jung J, Rojas JP, Al-Nawas B. Dynamic contrast-enhanced magnetic resonance imaging for monitoring neovascularization during bone regeneration-a randomized in vivo study in rabbits. Clin Oral Investig 2021;25:5843-54.
29. Qi XL, Burns P, Hong J, Stainsby J, Wright G. Characterizing blood volume fraction (BVF) in a VX2 tumor. Magn Reson Imaging 2008;26:206-14.
30. Bennett RE, Robbins AB, Hu M, Cao X, Betensky RA, Clark T, Das S, Hyman BT. Tau induces blood vessel abnormalities and angiogenesis-related gene expression in P301L transgenic mice and human Alzheimer's disease. Proc Natl Acad Sci U S A 2018;115:E1289-98.
31. Fischer VW, Siddiqi A, Yusufaly Y. Altered angioarchitecture in selected areas of brains with Alzheimer's disease. Acta Neuropathol 1990;79:672-9.
32. Ielacqua GD, Schlegel F, Füchtemeier M, Xandry J, Rudin M, Klohs J. Magnetic Resonance Q Mapping Reveals a Decrease in Microvessel Density in the arcAβ Mouse Model of Cerebral Amyloidosis. Front Aging Neurosci 2016;7:241.
33. Collette F, Hogge M, Salmon E, Van der Linden M. Exploration of the neural substrates of executive functioning by functional neuroimaging. Neuroscience 2006;139:209-21.
34. Zhang X, Yin X, Zhang J, Li A, Gong H, Luo Q, Zhang H, Gao Z, Jiang H. High-resolution mapping of brain vasculature and its impairment in the hippocampus of Alzheimer's disease mice. Natl Sci Rev 2019;6:1223-38.
35. Weller RO, Boche D, Nicoll JA. Microvasculature changes and cerebral amyloid angiopathy in Alzheimer's disease and their potential impact on therapy. Acta Neuropathol 2009;118:87-102.
36. Merlini M, Wanner D, Nitsch RM. Tau pathology-dependent remodelling of cerebral arteries precedes Alzheimer's disease-related microvascular cerebral amyloid angiopathy. Acta Neuropathol 2016;131:737-52.
37. van Gijn J. Leukoaraiosis and vascular dementia. Neurology 1998;51:S3-8.
38. Haller S, Kövari E, Herrmann FR, Cuvinciuc V, Tomm AM, Zulian GB, Lovblad KO, Giannakopoulos P, Bouras C. Do brain T2/FLAIR white matter hyperintensities correspond to myelin loss in normal aging? A radiologic-neuropathologic correlation study. Acta Neuropathol

Commun 2013;1:14.
39. Block ML, Zecca L, Hong JS. Microglia-mediated neurotoxicity: uncovering the molecular mechanisms. Nat Rev Neurosci 2007;8:57-69.
40. Cuello AC. Early and Late CNS Inflammation in Alzheimer's Disease: Two Extremes of a Continuum? Trends Pharmacol Sci 2017;38:956-66.

Cite this article as: Guo XY, Kwon HJ, Rhee HY, Park S, Cho AR, Ryu CW, Jahng GH. Microvascular morphology alteration using relaxation rate change with gadolinium-based magnetic resonance imaging contrast agent in patients with Alzheimer's disease. Quant Imaging Med Surg 2023;13(1):1-16. doi: 10.21037/qims-22-524

Supplementary

Table S1 Results of the voxel-based comparisons of microvascular indices between the participant groups

Group analysis	Cluster size	Cluster location	BA	Talairach coordinates	Z score
ADC					
CN<AD					
	665	Lt Parahippocampal Gyrus		-28.42,-5.31,-25.98	4.037
		Lt Temporal Lobe Sub-Gyral		-32.71,-2.14,-14.95	3.273
		Lt Uncus	28	-24.23,-12.06,-29.26	3.191
	868	Rt Temporal Lobe Sub-Gyral		51.72,-42.76,-6.56	3.940
		Rt Fusiform Gyrus		42.12,-44.59,-16.35	3.672
		Rt Superior Temporal Gyrus		47.36,-37.32,10.1	3.340
	881	Rt Parahippocampal Gyrus	27	18.35,-37.52,-1.22	3.895
		Rt Amygdala		25.56,-6.77,-13.05	3.741
	305	Rt Middle Temporal Gyrus	21	50.64,-4.85,-19.2	3.812
		Rt Temporal Lobe Sub-Gyral		46.47,-11.68,-21.27	3.311
	194	Lt Cerebellum Declive		-9.43,-70.39,-10.21	3.795
	216	Rt Superior Temporal Gyrus	22	46.22,-16.31,-2.79	3.734
	213	Rt Inferior Parietal Lobule	40	54.11,-45.64,22.94	3.603
		Rt Superior Temporal Gyrus		45.78,-52.46,20.8	3.435
	95	Rt Middle Temporal Gyrus		54.6,-24.21,-8.8	3.560
	98	Lt Superior Occipital Gyrus	19	-36.37,-81.29,30.19	3.493
		Lt Angular Gyrus	39	-46.06,-72.85,30.83	3.351
	75	Rt Frontal Lobe Sub-Gyral		33.33,10.97,36.06	3.488
	93	Rt Brainstem		11.65,-12.42,-12.47	3.440
	135	Lt Middle Temporal Gyrus	39	-41.65,-76.5,10.29	3.423
		Lt Middle Occipital Gyrus		-41.51,-76.86,-0.55	3.394
	55	Lt Posterior Cingulate		-15.2,-61.01,9.5	3.305
BVf					
CN<AD					
	236	Lt Precentral Gyrus		-30.74,-16.29,43.2	3.640
		Lt Parietal Lobe Sub-Gyral		-36.34,-30.37,43.13	3.164
	68	Lt Frontal Lobe Sub-Gyral		-18.45,-23.38,57.6	3.595
	152	Lt Thalamus Pulvinar		-13.68,-23.02,10.42	3.581
		Lt Thalamus Ventral Lateral Nucleus		-17.89,-13.74,16.64	3.494
	59	Rt Cerebellum Pyramis		24.16,-79.52,-33.48	3.552
mVD					
CN>AD	639	Lt Medial Frontal Gyrus	10	-11.8,45,-7.42	4.108
	318	Rt Medial Frontal Gyrus		7.51,59.09,6.4	4.016
	440	Rt Medial Frontal Gyrus		10.44,52,-7.74	3.939
		Rt Frontal Lobe Sub-Gyral		13.23,41.07,-11.43	3.379
	165	Rt Middle Frontal Gyrus		33.98,48.69,-3.6	3.908
	134	Lt Cingulate Gyrus		-6.77,32.93,29.35	3.701
	85	Lt Medial Frontal Gyrus		-7.83,58.65,11.5	3.385
VSI CN>AD					
	1668	Lt Medial Frontal Gyrus	10	-9.02,49.18,-6.98	4.865
		Inter-Hemispheric Corpus Callosum		0.53,24.59,-1.04	4.143
		Rt Anterior Cingulate		7.46,40.93,4.68	3.737
	347	Lt Cerebellum Tuber		-43.92,-61.78,-24.84	4.208
	448	Lt Cerebellum Declive		-16.27,-84.68,-22.49	4.102
	191	Lt Cingulate Gyrus	24	-1.59,-4.13,47.55	4.002
	245	Lt Cingulate Gyrus	32	-9.55,31.54,29.18	3.930
	302	Rt Medial Frontal Gyrus		7.51,59.09,6.4	3.745
	98	Rt Corpus Callosum		12.59,-37.66,14.89	3.634
	73	Rt Middle Frontal Gyrus		39.51,32.02,-6.43	3.387
MvWI					
CN<AD	664	Rt Frontal Lobe Sub-Gyral		29.16,2.74,33.86	3.990
		Rt Middle Frontal Gyrus		30.5,10.6,40.03	3.785
	173	Lt Extra-Nuclear		-21.69,-2.86,-8.07	3.841
	376	Lt Parietal Lobe Sub-Gyral		-28.02,-53.77,36.99	3.691
	204	Lt Middle Frontal Gyrus		-29.35,-12.24,44.96	3.567
	65	Rt Precentral Gyrus		21.76,-21.19,62.54	3.516
	117	Rt Medial Frontal Gyrus		8.44,43.37,37.36	3.401
	118	Lt Extra-Nuclear		-25.98,-22.92,-4.64	3.352
	52	Rt Temporal Lobe Sub-Gyral		49.26,-2.05,-18.96	3.244
GMV					
CN>AD	2207	Rt Caudate Tail		32.14,-34.6,6.95	4.953
		Rt Thalamus		29.45,-29.87,1.95	4.934
	1477	Lt Thalamus		-26.04,-27.93,-1.51	4.403
		Lt Parahippocampal Gyrus	27,28	-20.38,-27.17,-9.45	4.264
	203	Rt Medial Frontal Gyrus	8	12.54,36.95,40.42	4.105
	227	Rt Cuneus	17	23.69,-76.61,4.18	4.099
	111	Lt Superior Temporal Gyrus	13	-44.43,-45.43,19.49	3.980
	530	Rt Middle Temporal Gyrus	21	50.43,-27.41,-9.63	3.830
		Rt Temporal Lobe Sub-Gyral	20	46.43,-17.96,-19.61	3.696
		Rt Inferior Temporal Gyrus	20	50.56,-25.1,-18.87	3.475
	598	Rt Temporal Lobe Sub-Gyral	39	30.39,-61.97,27.3	3.803
		Rt Precuneus	7	20.6,-61.04,32.62	3.740
	89	Lt Insula	13	-34.37,26.97,14.36	3.443
		Lt Middle Frontal Gyrus	10	-32.91,34.34,11.03	3.234
WMV					
CN>AD	472	Lt Cerebellum Tuber		-16.22,-87.5,-27.26	4.677
	245	Lt Superior Frontal Gyrus	6	-7.18,23.91,59.12	3.810
	661	Lt Cerebellum Tuber		-46.64,-57.74,-27.66	3.783
		Lt Cerebellum Cerebellar Tonsil		-42.33,-59.38,-39.9	3.641
		Lt Cerebellum Culmen		-45.22,-49.23,-28.18	3.387

Rt, right; Lt, Lt; BA, Brodmann area. P=0.001 without multiple comparison and 50 voxels, age as covariates. CN, cognitively normal; AD, Alzheimer's disease; ADC, apparent diffusion coefficient; BVf, blood volume fraction; mVD, mean vessel diameter; VSI, vessel size index; MvWI, microvessel-weighted imaging; GMV, gray matter volume; WMV, white matter volume.

https://dx.doi.org/10.21037/qims-22-524

Table S2 Results of the voxel-based multiple regression analyses between microvascular indices and age

Group analysis	Cluster size	Cluster location	BA	Talairach coordinates	Z score
ADC					
(+) Age	18063	Lt Corpus Callosum		-10.55,27.57,-2.3	5.070
		Rt Extra-Nuclear		32.46,-8.46,-10.39	4.877
		Rt Lateral Ventricle		35.16,-17.26,-7.12	4.835
	6966	Lt Superior Temporal Gyrus	38	-31.1,15.92,-26.72	4.869
		Lt Middle Temporal Gyrus		-49.21,-0.88,-27.27	4.644
		Lt Temporal Lobe Sub-Gyral		-38.13,-2.47,-25.88	4.599
	888	Lt Precuneus		-29.48,-59.75,40.46	4.757
		Lt Inferior Parietal Lobule	40	-36.42,-54.25,42.21	3.613
		Lt Angular Gyrus		-37.71,-61.72,32.02	3.295
	637	Rt Insula	13	43.52,14.45,0.08	4.602
	1440	Lt Anterior Cingulate		-1.08,36.61,20.34	4.251
		Lt Medial Frontal Gyrus	6,9	-16.48,34.37,29.33	3.965
	268	Lt Cerebellum Culmen		-42.47,-46.29,-24.7	3.338
	261	Lt Middle Temporal Gyrus		-56.45,-35.95,-14.5	3.811
	224	Lt Inferior Parietal Lobule		-45.96,-30.93,34.8	3.809
		Lt Supramarginal Gyrus		-44.61,-39.45,35.37	3.802
	65	Lt Cerebellum Pyramis		-23.08,-82.33,-31.84	3.660
	593	Lt Cerebellum Declive		-30.16,-76.48,-19.24	3.616
		Lt Middle Temporal Gyrus		-40.15,-62.01,6.28	3.599
		Lt Occipital Lobe Sub-Gyral		-37.21,-64.92,-7.46	3.545
	66	Rt Middle Temporal Gyrus		45.21,2.95,-26.66	3.561
	78	Lt Precentral Gyrus	6	-40.31,-6.94,34.47	3.543
	175	Rt Cerebellum Declive		47.65,-59.86,-19.05	3.396
		Rt Cerebellum Tuber		51.9,-52.37,-23.68	3.302
	101	Lt Middle Frontal Gyrus	9	-37.36,25.84,30.87	3.384
		Lt Precentral Gyrus		-36.07,20.98,37.18	3.337
BVf (+) Age					
	95	Rt Lateral Ventricle		29.61,-17.23,-7.21	3.691
	58	Rt Middle Temporal Gyrus		61.55,-37.83,-14.03	3.618
	102	Lt CerebellumTuber		-27.28,-77.11,-27.36	3.499
	98	Rt Middle Frontal Gyrus		37.71,35.88,26.33	3.477
	100	Lt Middle Occipital Gyrus		-23.72,-89.83,16.09	3.458
		Lt Cuneus	18	-14.04,-90.14,18.92	3.145
	80	Rt Frontal Lobe Sub-Gyral		44.63,15.15,21.78	3.425
	57	Lt Cuneus	17	-2.71,-95.35,-0.3	3.382
	51	Rt Temporal Lobe Sub-Gyral		27.63,-70.92,22.8	3.344
	50	Lt Cingulate Gyrus	24,32	-5.48,12.96,31.54	3.251
ΔR2					
(+) Age	3980	Rt Extra-Nuclear		28.08,14.62,13.34	4.263
		Rt Insula		32.21,2.02,12.22	4.110
		Rt Lentiform Nucleus Putamen		25.4,-2.49,0.87	4.019
	439	Rt Superior Temporal Gyrus		50.43,-13.27,-5.14	4.187
		Rt Middle Temporal Gyrus		60.01,-30.75,0.13	3.555
	98	Lt Middle Occipital Gyrus		-30.71,-85.99,20.38	3.881
	393	Lt Frontal Lobe Sub-Gyral		-19.22,15.48,20.73	3.829
	192	Rt Frontal Lobe Sub-Gyral		31.98,5.78,31.49	3.825
	130	Lt Extra-Nuclear		-22.16,-40.53,16.73	3.788
		Lt Lateral Ventricle		-30.36,-46.43,5.22	3.487
	162	Lt Lateral Ventricle		-35.68,-28.2,-8.01	3.775
		Lt Lateral Ventricle		-27.27,-18.07,-10.96	3.422
		Lt Lateral Ventricle		-34.16,-13.58,-13.35	3.365
	96	Lt Cerebellum Declive		-1.04,-67.24,-13.82	3.769
	93	Rt Inferior Frontal Gyrus		40.92,29.48,-9.35	3.767
	53	Lt Middle Temporal Gyrus	21	-64.91,-25.91,-1.53	3.702
	142	Lt Lateral Ventricle		-5.4,-2.89,20.58	3.696
		Lt Corpus Callosum		-9.64,-10.25,23.86	3.396
		Lt Lateral Ventricle		-2.55,4.47,17.27	3.358
	144	Lt Cerebellum Culmen		-2.54,-48.85,0.06	3.682
	325	Rt Middle Frontal Gyrus		36.39,36.41,20.95	3.627
		Rt Middle Frontal Gyrus		43.31,32.05,22.01	3.623
		Rt Frontal Lobe Sub-Gyral		40.46,24.69,25.32	3.577
	300	Rt Frontal Lobe Sub-Gyral		21.51,37.97,-8.88	3.624
		Rt Frontal Lobe Sub-Gyral		22.9,22.85,-12.99	3.598
		Rt Frontal Lobe Sub-Gyral		18.77,46.5,-9.47	3.466
	77	Lt Insula	40	-48.45,-23.37,15.21	3.586
	199	Lt Inferior Frontal Gyrus		-32.65,33.93,-8.83	3.505
		Lt Frontal Lobe Sub-Gyral		-21.52,25.88,-13.45	3.234
		Lt Frontal Lobe Sub-Gyral		-14.6,21.52,-12.4	3.212
	63	Rt Posterior Cingulate	31	18.02,-66.03,16.34	3.452
	75	Lt Frontal Lobe Sub-Gyral		-35.8,16.09,15.11	3.447
	143	Rt Corpus Callosum		4.22,-18.7,23.3	3.428
		Rt Lateral Ventricle		15.33,-37.93,17.61	3.372
		Lt Extra-Nuclear		-1.28,-26.54,17.06	3.300
	68	Rt Temporal Lobe Sub-Gyral		47.4,-43.91,5.42	3.374
Q(+) Age					
	665	Rt Corpus Callosum		4.24,-26.83,19.82	3.867
		Rt Lateral Ventricle		15.33,-37.93,17.61	3.780
	116	Rt Superior Temporal Gyrus	38	52.09,12.04,-18.92	3.858
	246	Rt Middle Temporal Gyrus		54.59,-11.9,-4.93	3.767
		Rt Superior Temporal Gyrus		51.88,-1.84,-6.73	3.321
	64	Lt Middle Frontal Gyrus		-37.14,38.45,17.2	3.747
	75	Rt Inferior Frontal Gyrus		21.6,18.05,-21.57	3.693
	436	Rt Temporal Lobe Sub-Gyral		46.11,-30.8,1.24	3.643
		Rt Lateral Ventricle		37.94,-25.52,-9.21	3.366
	136	Lt Extra-Nuclear		-23.27,19.08,12.9	3.359
	93	Lt Inferior Frontal Gyrus	47	-24.31,12.05,-16.16	3.326
mVD					
(-) Age	286	Rt Medial Frontal Gyrus		7.7,23.45,-18.59	3.846
		Rt Inferior Frontal Gyrus	47	21.54,23.12,-15.69	3.293
	359	Lt Corpus Callosum		-3.63,24.61,-1.11	3.785
	71	Lt Frontal Lobe Sub-Gyral		-20.11,47.97,-8.63	3.529
	104	Rt Frontal Lobe Sub-Gyral		21.53,43.56,-8.35	3.382
		Rt Anterior Cingulate		13.13,45.87,-2.87	3.250
MvWI(+) Age					
	9841	Rt Lentiform Nucleus Putamen		21.33,2.38,-5.5	5.009
		Rt Extra-Nuclear		21.03,0.16,17.26	4.119
	1478	Lt Middle Frontal Gyrus		-39.79,53.09,11.79	4.607
		Lt Superior Frontal Gyrus		-35.78,51.9,23.9	3.967
		Lt Inferior Frontal Gyrus		-45.19,44.65,-2.62	3.437
	9722	Lt Caudate Head		-13.43,13.09,1.69	4.485
		Lt Superior Temporal Gyrus		-52.15,10.27,-11.4	4.317
		Lt Insula	13	-41.21,-14.33,-5.43	4.176
	854	Lt Middle Frontal Gyrus		-36.02,14.52,31.17	3.718
	276	Rt Brainstem		12.93,-26.92,-8.41	3.680
	118	Lt Middle Frontal Gyrus	6	-30.71,-5.11,44.26	3.613
	213	Rt Temporal Lobe Sub-Gyral		47.45,-43.52,1.41	3.536
	110	Lt Thalamus	Pulvinar	-9.47,-25.45,6.21	3.510
	177	Rt Middle Frontal Gyrus	6	32.99,9.89,61.62	3.507
	74	Lt Superior Frontal Gyrus	8	-19.38,48.58,42.78	3.491
	205	Rt Inferior Temporal Gyrus		41.81,-71.57,0.01	3.488
		Rt Middle Temporal Gyrus	37	44.55,-64.99,4.73	3.242
	67	Rt Lingual Gyrus	18	7.16,-84.71,-8.58	3.463
	54	Lt Cerebellum Declive		-20.33,-60.64,-22.98	3.416
	56	Rt Middle Frontal Gyrus		42.33,36.46,-8.67	3.406
	71	Rt Corpus Callosum		4.45,22.73,17.77	3.385
	97	Lt Temporal Lobe Sub-Gyral		-37.13,-34.17,-4.54	3.321
	66	Lt Parietal Lobe Sub-Gyral		-36.13,-43.91,22.93	3.313
	59	Lt Thalamus Anterior Nucleus		-5.27,-6.04,9.47	3.306
	50	Lt Medial Frontal Gyrus		-6.25,24.4,-13.34	3.273
	53	Lt Insula	13	-41.35,10.66,13.15	3.224
GMV(-) Age					
	2996	Lt Superior Frontal Gyrus	10	-11.77,55.75,-6.86	5.325
		Lt Middle Frontal Gyrus	10	-20.41,61.7,19.24	3.891
	2822	No Gray Matter found		-8.95,5.34,-25.1	3.969
		Lt Parahippocampal Gyrus	Hippocampus	-27.22,-14.04,-13.73	3.856
		Lt Parahippocampal Gyrus	28	-14.73,-8.64,-11.65	3.551
	87	Rt Inferior Frontal Gyrus	9	54.36,21.53,23.45	3.840
	404	Lt Cuneus	18	-11.16,-78.87,14.18	3.811
		Lt Posterior Cingulate	30	-11.04,-65.64,8.68	3.518
	938	Rt CerebellumCulmen		38.04,-48.53,-24	3.775
	1391	Rt Inferior Frontal Gyrus	47	13.25,9.29,-23	3.682
		Rt Superior Temporal Gyrus	38	31.4,7.18,-31	3.680
		Rt Uncus	28	13.35,4.48,-31.56	3.505
	232	Lt Parahippocampal Gyrus	19,30	-20.59,-54.77,-1.26	3.645
	77	Rt Thalamus Pulvinar		5.69,-36.39,11.74	3.567
	132	Lt Cingulate Gyrus	24	-6.88,12.42,32.36	3.468
		Lt Anterior Cingulate	24	-6.76,21.59,25.13	3.128
	233	Rt Parahippocampal Gyrus	35	21.48,-23.02,-24.57	3.418
		Rt CerebellumCulmen		21.33,-33.72,-16.12	3.273
	69	Lt Superior Temporal Gyrus	38	-36.69,12.47,-24.89	3.254
WMV (-) Age					
	1028	Lt Parahippocampal Gyrus		-38.31,-34.42,-21.25	4.856
		Lt Fusiform Gyrus		-39.77,-41.79,-17.92	4.238
	88	Lt Middle Temporal Gyrus		-41.81,-74.04,23.58	3.879
	1485	Lt Superior Frontal Gyrus		-21.74,52.58,11.59	3.836
		Lt Medial Frontal Gyrus		-7.86,51.11,11.69	3.534

Rt, right; Lt, Lt; BA, Brodmann area (+) indicates the positive correlation; (-) indicates the negative correlation. P=0.001 without multiple comparison and 50 voxels. CN, cognitively normal; AD, Alzheimer's disease; ADC, apparent diffusion coefficient; BVf, blood volume fraction; Q, mean vessel density; mVD, mean vessel diameter; MvWI, microvessel-weighted imaging; GMV, gray matter volume; WMV, white matter volume.

https://dx.doi.org/10.21037/qims-22-524

Table S3 Results of comparisons of apparent diffusion coefficient (ADC), ΔR2, ΔR2*, gray matter volume (GMV), and white matter volume (WMV) between the participant groups in specific brain areas and results of association between each microvascular index and the disease group and age

Microvascular Index	ROI	CN	AD	*P-value/ z-value	#F/p (group-p/age-p)
ADC×10^3 (mm^2/s)	Hippocampus	1.128(1.076 to 1.208)	1.374 (1.261 to 1.431)	<0.001*/3.382	F=21.220/p<0.001* (0.004*/0.009*)
	Parahippocampal Gyrus	1.082 (1.057 to 1.100)	1.238 (1.209 to 1.266)	<0.001*/ 3.710	F=22.764/p=<0.001* (0.001*/0.035*)
	Precuneus	1.038 (0.995 to 1.096)	1.115 (1.068 to 1.183)	0.017*/ 2.397	F=4.574/p= 0.024* (0.093/0.304)
	Caduate	1.354 (1.289 to 1.433)	1.404 (1.295 to 1.540)	0.577/ 0.558	F=2.800/p=0.086 (0.463/0.034*)
	Corpus callosum	1.413 (1.382 to 1.445)	1.573 (1.480 to 1.655)	0.005*/ 2.791	F=5.807/p=0.011* (0.067/0.226)
	Globus Pallidus	0.669 (0.645 to 0.740)	0.755 (0.681 to 0.847)	0.020*/ 2.331	F=2.210/p= 0.137 (0.102/0.960)
	Lateral Ventricle	1.661 (1.620 to 1.688)	1.775 (1.699 to 1.831)	0.024*/ 2.265	F=11.920/p=<0.001* (0.659/0.001*)
	Putamen	0.723 (0.657 to 0.757)	0.754 (0.723 to 0.935)	0.094/ 1.674	F=1.277/p= 0.302 (0.305/0.683)
	Thalamus	1.099 (1.044 to 1.124)	1.142 (1.010 to 1.192)	0.224/ 1.215	F=1.190/p= 0.326 (0.739/0.166)
	GMV70	1.008 (0.949 to 1.056)	1.120 (1.034 to 1.202)	0.033*/ 2.134	F=5.060/p=0.017* (0.398/0.053)
	WMV70	0.962 (0.924 to 0.993)	1.077 (0.988 to 1.124)	0.012*/ 2.528	F=1.062/p= 0.366 (0.172/0.302)
	WMHI	1.124 (1.095 to 1.252)	1.200 (1.111 to 1.291)	0.412/ 0.821	F=4.584/p=0.024* (0.158/0.182)
ΔR2 (1/s)	Hippocampus	0.477 (0.044 to 0.755)	0.389 (0.046 to 1.132)	0.922/ 0.099	F=6.084/p=0.009* (0.122/0.003*)
	Parahippocampal Gyrus	0.350 (-0.021 to 0.764)	-0.005 (-0.347 to 0.848)	0.577/ 0.558	F=3.721/p=0.043* (0.062/0.016*)
	Precuneus	0.500 (0.070 to 0.985)	0.335 (0.018 to 0.971)	0.670/ 0.427	F=2.687/p=0.094 (0.178/0.032*)
	Caduate	0.361 (0.042 to 1.171)	0.395 (-0.067 to 1.734)	0.818/ 0.230	F=0.084/p=0.919 (0.702/0.746)
	Corpus callosum	0.381 (-0.050 to 0.649)	-0.019 (-0.366 to 1.100)	0.622/ 0.492	F=4.621/p=0.023* (0.103/0.007*)
	Globus Pallidus	0.382 (-0.136 to 0.799)	0.335 (-0.247 to 1.050)	0.870/ 0.164	F=1.089/p=0.357 (0.577/0.164)
	Lateral Ventricle	0.427 (0.015 to 0.898)	0.434 (0.095 to 1.079)	0.870/ 0.164	F=4.273/p=0.029* (0.250/0.010*)
	Putamen	0.375 (-0.207 to 0.742)	0.172 (-0.445 to 1.143)	0.922/ 0.099	F=2.094/p=0.151 (0.422/0.058)
	Thalamus	0.696 (0.290 to 1.013)	0.441 (-0.004 to 1.306)	0.622/ 0.492	F=0.284/p=0.756 (0.462/0.647)
	GMV70	0.379 (-0.026 to 0.924)	0.635 (-0.005 to 1.049)	0.974/ 0.033	F=2.983/p=0.075 (0.201/0.025*)
	WMV70	0.370 (-0.046 to 0.902)	0.039 (-0.385 to 0.863)	0.412/ 0.821	F=3.396/p=0.055 (0.091/0.019*)
	WMHI	0.606 (0.019 to 0.819)	0.139 (0.008 to 0.861)	0.577/ 0.558	F=2.726/p=0.091 (0.237/0.031*)
ΔR2* (1/s)	Hippocampus	2.516 (1.210 to 4.763)	2.666 (1.768 to 3.360)	0.922/ 0.099	F=0.016/p=0.984 (0.898/0.977)
	Parahippocampal Gyrus	1.824 (0.778 to 3.384)	1.800 (1.060 to 2.357)	0.718/ 0.361	F=0.205/p=0.817 (0.532/0.687)
	Precuneus	1.877 (0.924 to 2.368)	1.457 (1.183 to 2.777)	0.922/ 0.099	F=0.218/p=0.806 (0.614/0.536)
	Caduate	2.378 (0.478 to 2.957)	1.357 (0.104 to 3.127)	0.577/ 0.558	F=0.701/p=0.509 (0.921/0.366)
	Corpus callosum	2.061 (0.381 to 2.402)	1.529 (1.340 to 2.492)	0.870/ 0.164	F=0.139/p=0.871 (0.623/0.681)
	Globus Pallidus	1.203 (0.458 to 3.624)	2.504 (0.561 to 4.794)	0.341/ 0.952	F=0.896/p=0.425 (0.239/0.269)
	Lateral Ventricle	2.143 (0.938 to 2.975)	1.613 (1.183 to 2.548)	0.577/ 0.558	F=0.995/p=0.388 (0.970/0.247)
	Putamen	1.350 (0.629 to 3.016)	1.294 (0.878 to 2.984)	0.974/ 0.033	F=0.066/p=0.936 (0.906/0.728)
	Thalamus	1.837 (0.920 to 2.712)	2.434 (1.164 to 3.327)	0.412/ 0.821	F=0.619/p=0.549 (0.280/0.528)
	GMV70	2.042 (1.070 to 2.837)	2.043 (1.533 to 2.802)	0.670/ 0.427	F=1.063/p=0.365 (0.906/0.218)
	WMV70	1.546 (1.023 to 2.004)	1.491 (1.036 to 2.095)	0.768/ 0.295	F=0.097/p=0.908 (0.917/0.770)
	WMHI	1.081 (0.600 to 1.734)	1.027 (0.378 to 2.059)	0.870/ 0.164	F=0.165/p=0.849 (0.856/0.729)
GMV (mm^3)	Hippocampus	0.420 (0.395 to 0.444)	0.282 (0.259 to 0.352)	<0.001*/ 3.447	N/A
	Parahippocampal Gyrus	0.392 (0.356 to 0.430)	0.295 (0.282 to 0.343)	<0.001*/ 3.316	N/A
	Precuneus	0.296 (0.275 to 0.308)	0.257 (0.242 to 0.288)	0.028*/ 2.200	N/A
	Caduate	0.307 (0.271 to 0.317)	0.300 (0.250 to 0.336)	0.533/ 0.624	N/A
	Corpus callosum	0.111 (0.104 to 0.117)	0.115 (0.107 to 0.121)	0.450/ 0.755	N/A
	Globus Pallidus	0.157 (0.144 to 0.173)	0.157 (0.130 to 0.170)	0.412/ 0.821	N/A
	Lateral Ventricle	0.148 (0.143 to 0.159)	0.140 (0. 125 to 0.146)	0.039*/ 2.068	N/A
	Putamen	0.326 (0.311 to 0.373)	0.332 (0.291 to 0.354)	0.670/ 0.427	N/A
	Thalamus	0.341 (0.306 to 0.375)	0.320 (0.287 to 0.362)	0.309/ 1.018	N/A
WMV (mm^3)	Hippocampus	0.197 (0.190 to 0.232)	0.190 (0.153 to 0.210)	0.158/ 1.412	N/A
	Parahippocampal Gyrus	0.188 (0.169 to 0.213)	0.176 (0.144 to 0.191)	0.123/ 1.543	N/A
	Precuneus	0.214 (0.192 to 0.253)	0.214 (0.191 to 0.240)	0.768/ 0.295	N/A
	Caduate	0.160 (0.148 to 0.176)	0.171 (0.155 to 0.192)	0.375/ 0.886	N/A
	Corpus callosum	0.368 (0.332 to 0.427)	0.368 (0.332 to 0.427)	0.450/ 0.755	N/A
	Globus Pallidus	0.436 (0.412 to 0.521)	0.483 (0.384 to 0.516)	0.974/ 0.031	N/A
	Lateral Ventricle	0.245 (0.223 to 0.261)	0.236 (0.213 to 0.273)	0.670/ 0.427	N/A
	Putamen	0.288 (0.276 to 0.341)	0.306 (0.275 to 0.320)	0.622/ 0.492	N/A
	Thalamus	0.197 (0.191 to 0.255)	0.228 (0.191 to 0.249)	0.577/ 0.558	N/A

*, P-value by Mann-Whitney U-test and data are listed as median (95% CI for the median). #, F and P-values by multiple regression analysis with modeling as each microvascular index = participant group + age. CN, cognitively normal; AD, Alzheimer's disease; ROI, region-of-interest; GMV70, 70% gray matter volume; WMV70, 70% white matter volume; WMHI, white matter hyperintensity.

https://dx.doi.org/10.21037/qims-22-524

Table S4 Results of correlation analyses between apparent diffusion coefficient (ADC), ΔR2, ΔR2*, gray matter volume (GMV), and white matter volume (WMV) and age or mini-mental state examination (MMSE) scores in specific brain areas

ROIs	Microvascular Index / Variable	ADC×10^3 (mm^2/s) rho/P value	ΔR2 (1/s) rho/ P value	ΔR2* (1/s) rho/ P value	GMV (mm^3) rho/P value	WMV (mm^3) rho/P value
Hippocampus	†age	0.701/<0.001*	0.560/0.007*	0.031/0.891	-0.654/0.001*	-0.634/0.002*
	*MMSE	-0.305/0.178	-0.004/0.985	-0.100/0.667	0.276/0.226	0.550/0.010*
Parahippocampal Gyrus	†age	0.714/<0.001*	0.384/0.077	0.093/0.680	-0.652/0.001*	-0.669/<0.001*
	*MMSE	-0.248/0.278	0.086/0.713	-0.121/0.601	0.252/0.271	0.595/0.004*
Precuneus	†age	0.452/0.035*	0.378/0.083	0.162/0.472	-0.242/0.290	-0.262/0.251
	*MMSE	0.056/0.809	0.104/0.652	0.085/0.716	0.321/0.157	0.488/0.025*
Caudate	†age	0.461/0.031*	0.260/0.243	-0.140/0.534	-0.122/0.598	-0.080/0.731
	*MMSE	0.045/0.848	-0.157/0.497	-0.109/0.638	-0.078/0.736	0.419/0.059
Corpus Callosum	†age	0.587/0.004*	0.508/0.016*	-0.021/0.926	-0.371/0.098	-0.402/0.071
	*MMSE	-0.055/0.811	-0.040/0.864	-0.145/0.530	-0.085/0.715	0.604/0.004*
Globus Pallidus	†age	0.514/0.014*	0.313/0.157	-0.077/0.734	-0.195/0.397	-0.320/0.158
	*MMSE	-0.022/0.925	-0.136/0.558	-0.209/0.363	0.053/0.819	0.355/0.114
Lateral Ventricle	†age	0.734/<0.001*	0.509/0.016*	-0.159/0.479	-0.447/0.042*	-0.435/0.049*
	*MMSE	-0.080/0.730	-0.031/0.894	-0.185/0.423	0.088/0.704	0.557/0.009*
Putamen	†age	0.343/0.119	0.394/0.070	0.035/0.879	-0.119/0.608	-0.398/0.074
	*MMSE	-0.045/0.840	-0.201/0.382	0.053/0.820	0.099/0.670	0.382/0.088
Thalamus	†age	0.474/0.026*	0.216/0.335	-0.051/0.822	-0.275/0.227	-0.148/0.521
	*MMSE	-0.135/0.561	-0.132/0.567	-0.206/0.371	-0.203/0.377	0.401/0.072
GMV70	†age	0.562/0.007*	0.481/0.023*	0.304/0.170		
	*MMSE	-0.063/0.787	0.009/0.968	-0.180/0.434		
WMV70	†age	0.490/0.021*	0.345/0.116	0.201/0.371		
	*MMSE	-0.214/0.352	-0.055/0.811	-0.411/0.064		
WMHI	†age	-0.159/0.479	0.358/0.102	0.153/0.498		
	*MMSE	-0.352/0.117	-0.059/0.798	-0.083/0.720		

†age: Rank correlation analysis (Spearman's coefficient /P value). *MMSE: Partial correlation analysis (rho/P value) with age as a covariate. GMV and WMV: partial correlation analysis (rho/P value) with both age and TIV as covariates. GMV70, 70% gray matter volume; WMV70, 70% white matter volume; WMHI, white matter hyperintensity.

https://dx.doi.org/10.21037/qims-22-524

Table S5 Results of paired comparisons of apparent diffusion coefficient (ADC), ΔR2, ΔR2* among 70% gray matter volume (GMV70), 70% white matter volume (WMV70), and WMHI ROIs in the cognitive normal (CN) or Alzheimer's disease (AD) participants

Microvascular Index	CN (P value)			AD (P value)		
	GMV70 *vs.* WMV70	GMV70 *vs.* WMHI	WMV70 *vs.* WMHI	GMV70 *vs.* WMV70	GMV70 *vs.* WMHI	WMV70 *vs.* WMHI
ADC×10^3	0.005*	<0.001*	0.001*	0.206	0.175	0.024*
DeltaR2	0.278	0.520	0.966	0.278	0.765	0.102
DeltaR2star	0.024*	0.024*	0.465	0.007*	0.005*	0.413

P value by Wilcoxon rank test analysis. WMHI, white matter hyperintensity.

https://dx.doi.org/10.21037/qims-22-524